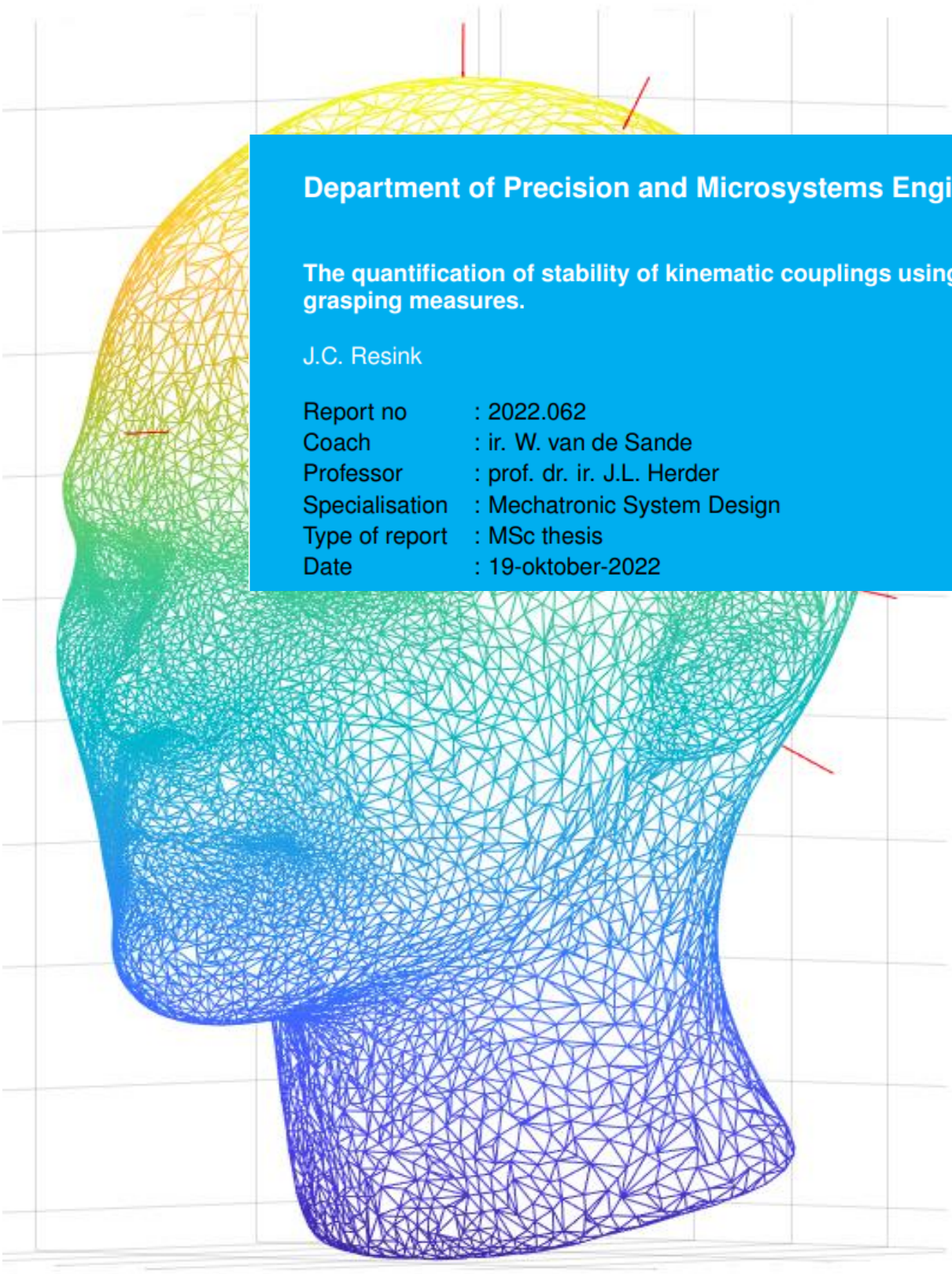

Department of Precision and Microsystems Engineering

The quantification of stability of kinematic couplings using robotic grasping measures.

J.C. Resink

Report no	: 2022.062
Coach	: ir. W. van de Sande
Professor	: prof. dr. ir. J.L. Herder
Specialisation	: Mechatronic System Design
Type of report	: MSc thesis
Date	: 19-oktober-2022

TU Delft Delft University of Technology

Challenge the future

The quantification of stability of kinematic couplings using robotic grasping measures.

by

J.C. Resink

to obtain the degree of Master of Science
at the Delft University of Technology,
to be defended publicly on Wednesday October 19, 2022 at 2:00 PM.

Student number:	4965620	
Thesis committee:	prof. dr. ir. J.L. Herder,	TU Delft
	ir. W.W.P.J. van de Sande,	TU Delft
	dr. M. Wiertlewski	TU Delft

An electronic version of this thesis is available at http://repository.tudelft.nl/.

Preface

This thesis was conducted as part of the master Mechanical Engineering at the faculty of 3ME of the Technical University of Delft. The thesis is the final part for completion of the track High-Tech Engineering, specialisation Mechatronic System Design, part of the Precision and Microsystems Engineering department.

The project was presented by the HollandPTC, located at the campus of the TU Delft. The goal of the thesis was to investigate the implementability of kinematic couplings for the design of a patient-specific head fixation.

The work titled "**Quantification of the stability of kinematic couplings using robotic grasping measures**", is presented as the result that explains the potential for robotic grasping theory to be implemented for the design of patient-specific kinematic couplings. This work is structured as follows; The paper will be presented first, which presents the findings of this research. The content from Appendix A is part of this research. The content from appendix B is part of the overall thesis work.

Contents

The quantification of stability of kinematic couplings using robotic grasping measures.

J.C. Resink, J.L. Herder, W.W.P.J. van de Sande

***Abstract*—Kinematic couplings (KCs) are a subclass of couplings known for reaching unmatched precision, through relatively simplistic designs. The 3-vee-groove and Kelvin clamp are the archetype designs, and are still being further investigated for their potential. One of the limiting factors in the field of kinematic couplings is the lack of proper knowledge on how to assure stability of newly designed couplings. In this paper, the theoretical gap between the field of robotic grasping and the field of kinematic coupling is researched. It is shown that by making small alterations in the way of modelling the design problem, one can lend the performance measures that are used in the field robotic grasping for quantification of grasp performance, and apply these on the design process of kinematic couplings. This allows a designer to quantify and predict performance of newly designed couplings. The measures analysed in this paper are compared and scored in a table, where a tool is presented to help guide future coupling designers in the process.**

1. Introduction

A kinematic coupling (KC) [1], is a type of coupling which is specifically designed for the inhibition of relative motion between the 2 subsystems that are typically part of a coupling. These subsystems, usually in the shape of plates, generally make use of specific geometry that cause the plates to be deterministically positioned in a desired manner relative to each other. The contact between the plates is assured by a so called nesting force [2], which clamps the 2 subsystems together.

Kinematic couplings are known for their sub-micrometer range precision through simplistic design. As a consequence, fabrication cost of these couplings is generally low, giving them an unmatched precision-versus-cost ratio. Already discussed by Maxwell [3], these traits have made them popular in the early measurement instrument industry, and later in the high-tech sector [4–8]. The application of Exact Constraint Design (ECD) is the primal factor in achieving these traits [9]. This design philosophy dictates that by pursuing a 1 to 1 ratio between constraints and degrees of freedom (DOFs), internal stresses can be mitigated [10]. This makes the behavior of a system more predictable. In the case of kinematic couplings, these constraints are typically applied by using point contacts, whom need the nesting force to reassure contact with the geometry of the other plate. There are 2 archetypes in this field, the 3-vee-groove and the Kelvin clamp. Particularly the 3-vee-groove is popular due to its symmetry and low fabrication cost. Various additional designs and features throughout the years have been based on this design [11–14]. Research within the field of couplings is mostly focused on 2 main topics. Firstly, the *deterministic dilemma* [15, 16] is a trade-off problem where the pursuit of infinitely small (exact constraint) point contacts also causes the loading capability to diminish drastically, which is undesired. The second topic is mitigation of the error motions whilst the system is being coupled [17, 18]. This is determined by examining the potential error motions that could lead to misalignment.

A limiting factor of the KC field is the lacking design freedom. Merely proving independency of constraints by solving for the null-space of the equilibrium equations is often suggested as viable and sufficient to reassure stability [15, 18–20]. This can be seen as a binary result however, only proving whether a coupling is indeed exact constraint and at least marginally stable.

Another field where the ECD philosophy plays a role is called robotic grasping (RG). This field is focused on the grasping and manipulation of objects using robotic manipulators, also known as grippers.

The challenge of this field is how to assure a proper grip on randomly shaped polygons or polyhedron. This is a complex problem as discussed by Shimoga [21], where both variance in object as well as gripper [22–25] need to be addressed. Similarly to coupling literature, the basis of this field formed around the question of the minimum requirements in order to constraint an object in 2d [26] and 3d [27] resp. The modelling of the contacts plays a vital role in these requirements [28–30].

Like Baker mentioned, ”stability alone is not enough” [31]. Grasping is often modelled under the assumption that an object will be disturbed, either through manipulation or otherwise. Therefore, it is important to be able to quantify to what extent a certain grasp is able to withstand the disturbances. Screw theory was early suggested for this purpose, and is to this day still the most popular method for analysis [32].

By making use of so called *quality measures*, performance can be quantified based on different aspects of the grasp, depending on the measure. The best known method is suggested by Ferrari & Canny [33]. Their closest facet measure has been used throughout literature as benchmark for the relative performance of other suggested measures [34–37], and it has been used as a reference multiple

times in articles discussing computational improvements regarding convex hull operations [38–40].

Convex hull theory has been a parallel topic of research next to grasping literature over the years and forms a core aspect of screw theory based measures [41–47]. Although improved significantly over the years, the computational effort often still poses a bottleneck for these measures. This can be seen in the shift of focus of grasping research of the past few years towards better optimized algorithms to calculate already existing measures [38, 40, 48]. The following reviews give a proper overview of available measures and how they can be efficiently computed [21, 48–52].

The scope of this paper is first to explain the difference in design philosophy of robotic grasping measures compared to kinematic coupling theory. This is done in order to gain a better understanding of the underlying differences in their fundamental theory. The second goal of this paper is to show that these differences can be bridged, and that the measures from robotic grasping can be utilized to better analyse and predict performance of newly designed couplings.

The work is structured as follows; Firstly, section 2.1 will discuss the fundamental underlying theory of both fields, which will be compared relative to one another. The remaining part of section 2 will discuss background theory and used nomenclature and definitions for the remainder of this paper. Section 3 will discuss the criteria and the eventual selection of measures that are analysed, after which section 4 and 5 will discuss the measures themselves and how these will be implemented in a general performance study. The results of this general study will be presented in section 6, where a selection of the figures has been included in Appendix A for clarity. Section 7 analyses the performance of a newly suggested combined measure compared to a benchmark measure. The overall results of all measures is scored in section 8, after which the results are discussed in section 9. Section 10 will provide concluding remarks on this paper.

2. Fundamentals

In this section, fundamental theory that is being used in the next chapters is outlined.

2.1. Kinematics

Reuleaux is often considered the founding father of general constraint theory [53], which lies at the foundation of both coupling and grasping theory. In his book "Kinematics of machinery", it is geometrically deduced that in order to fully constrain objects in 2d, 4 contacts are required. The 3d case was quickly suggested [54], though the eventual prove presented by Lakshiminarayana was not presented until 80 years later [26]. Through the implementation of screw theory, it was now clear that for a 3 dimensional object, a minimum of 7 contacts is required in order for it to be fully constrained. This extra constraint compared to the amount of DOF is caused by the unilateral nature of the constraints. A single point contact is not capable of constraining a full dimension, but rather half of it. The reason that the amount of required contacts is not 6 and 12 for 2d and 3d resp, is caused by redundancy, where a point contacts can both constrain a partial translation as well as rotation.

In the work of Reuleaux the term *closing force* is stated as the force that is required to keep "element a in the place of a portion of the enveloping partner-element b". The corresponding figure is depicted in 1.

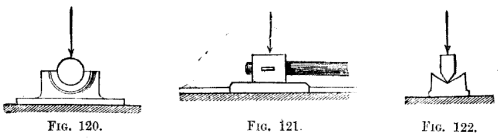

Figure 1: *Force closure*

It becomes clear that his definition shows remarkable resemblance with a point constraint. The 'closing force' term can be related to the local nesting force that Blanding later identified as a requirement for assuring contact between constraint and object [9], it is however, not treated as a constraint on itself. This seemingly innocent discrepancy lies at the heart of the difference in design philosophy of robotic grasping versus kinematic coupling. When looking at a kinematic coupling on system level, the required DOF that provides the coupling direction also assures that the contacts only span a half-space. This gives a coupling the distinct advantage that it can be loaded with 1 general nesting force, which acts as a preload force towards all contacts. It can be therefore concluded that the nesting force is considered part of the constraints. Maxwell's equation (1) thus holds for coupling design, where the contacts are treated as if they are bilateral of nature. This means that it is assumed that each constraint is capable of constraining the considered DOF in both positive as well as negative direction, despite being only a point contact.

$$DOF = 6 - C \tag{1}$$

Because of this approach, it becomes significantly easier to analyse the independency of the constraints, given that redundancy of constraints would result in an underconstrained design. A downside of this approach is that by generalizing the local forces into a general one, force distribution on a local level (per contact) becomes obscure. This explains why nesting forces are generally not defined in terms of magnitude. Local contact forces are an important aspect when considering the deterministic dilemma, given that the highest local loading force constrains the overall system loading capability.

To compare this with the approach from robotic grasping, the definition of Ponce regarding *force closure* can be best utilized [45]. This is a fundamental concept in robotic grasping, mathematically described in section 2.5. This definition states that the contacts of a grasp are force closed, if combined these contacts can deliver a force in any direction in 2d or 3d space.

This can be interpreted as the contacts interchangeably providing each other with a nesting force, rather than relying on a general one. This greatly relieves constraints

on modelling freedom, with the cost of making analysis less straightforward. Screw theory is generally used for these type of analysis. Although this theory is not always easy to incorporate, it has the distinct advantage that it is capable of analysing a system from both the perspective of degrees of freedom, as well as per constraint. This will be more elaborately explained in section 2.2. In general, the combination of these analysis holds the potential to be used to gain insight in both the force and moment distribution of a coupling, as well as the motion capabilities. It is therefore implemented in the design of couplings, given that both these aspects translate to key features that quantify the performance of a kinematic coupling.

2.2. Screw Theory

Often, the analysis regarding the quality of a grasp is done through the use of so called *screw theory*. Which is a dual theory that allows both moments and forces, and linear and angular velocities resp. to be analysed at the same time. Like Chasles' theorem states:

"Any motion of a rigid body in space may be described as a screw motion."

Which gives an idea on the versatility of screws. When one is interested in the constraint situation of a system, they look at the so called imposed *wrenches*. A wrench (2) represents the vector representation of the forces and moments that are imposed by a constraint on an object.

$$\vec{W} = \begin{bmatrix} \vec{f} \\ (\vec{r} \times \vec{f}) + q\vec{f} \end{bmatrix} = \begin{bmatrix} \vec{f} \\ \vec{\tau} \end{bmatrix} \tag{2}$$

Here, $\vec{f}$ is an orientation vector that indicates the axial force along the line of action of the wrench, $\vec{r}$ indicates the distance between the origin and some arbitrary point along this line, and a scalar constant q dictates the pitch. This pitch is the ratio between the axial force vs the torque of the wrench.

In some cases it can be of more or additional value to look at the freedom space of an object, which can be described using *twists* (3).

$$\vec{T} = \begin{bmatrix} \vec{\omega} \\ (\vec{c} \times \vec{\omega}) + p\vec{\omega} \end{bmatrix} = \begin{bmatrix} \vec{\omega} \\ \vec{v} \end{bmatrix} \tag{3}$$

Here, the velocity $\vec{\omega}$ can be considered dual to , $\vec{c}$ dual to $\vec{r}$ and p dual to q.

This duality between twists and wrenches offers an important tool for analysis. When a twist and a wrench are complementary or reciprocal to one another, their product will equal zero (2.2).

$$\vec{W} \cdot \vec{T} = \begin{bmatrix} \vec{f} & (\vec{r} \times \vec{f}) + q\vec{f} \end{bmatrix} \begin{bmatrix} (\vec{c} \times \vec{w}) + p\vec{w} \\ \vec{w} \end{bmatrix} = 0 \tag{4}$$

This means that no power is generated when a twist is under the influence of its reciprocal wrench. This tool can be used to investigate the effect of a constraint on a given motion.

2.3. Grasp matrix

Generally, when a grasp is analysed, the wrenches that are generated by the contact points on the object, known as the *primitive wrenches*, are combined into a single matrix known in RG literature as the *grasp matrix* [48, 55], in coupling nomenclature referred to as the *system matrix* [20]. There is an important distinction to be made here. Generally in analysis, the magnitudes of the contact forces are scaled to unity, which resembles the *G* matrix (5).

$$G = \begin{bmatrix} Fx_1 & Fx_2 & ... & Fx_n \\ Fy_1 & Fy_2 & ... & Fy_n \\ R_1 \times F_1 & R_2 \times F_2 & ... & R_n \times F_n \end{bmatrix} \tag{5}$$

with $|F| = 1$

for each contact however, it holds:

$$G_i f_i = \omega_i \tag{6}$$

Where each column of the G matrix can be scaled according to equation (6) by a magnitude f_i. In some cases it can be beneficial to scale it in accordance with the equilibrium force. The size of the *G* matrix becomes $\mathbb{R}^{m \times n}$, where m = 3 or m = 6, depending on whether the planar or spatial case is regarded.

2.4. Convex hull operations

A significant part of measures that will be discussed in this article is based on the so called *convex hull* (CH) of a particular matrix. A convex hull of a point set *P* describes the smallest subset *p*, such that all points of *P* are completely enclosed by *p*. The points making up the convex hull can be calculated using 2 distinct methods. A 2d simplification is depicted in figure 2.

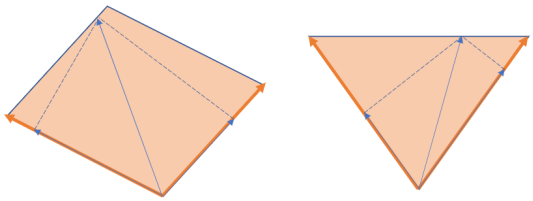

Figure 2: *Minkowski addition (l) Union addition (r)*

CH(*G*) is mathematically described in (7).

$$CH(G) = \sum_{i=1}^{n} \omega_i = \sum_{i=1}^{n} \sum_{j=1}^{m} \alpha_{ij} \omega_{ij} \tag{7}$$

with $\alpha_{ij} \geq 0$

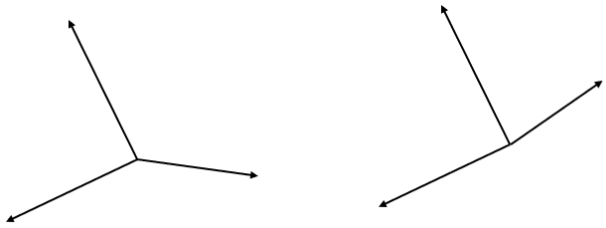

Figure 3: *positive span (L) vs non-positive span (R)*

Here, α_{ij} is the variation of the magnitude of the wrenches that make up the hull, and ω_i represents the column of the *G* matrix. Usually, either the combined sum of the primitive wrenches is limited, or the magnitude of the individual wrenches. This is known as taking the union or the minkowski sum of a matrix. Figure 2 shows the 2 approaches of constructing the hull of the wrenches. Mathematically described, the minkowski sum $\mathcal{M}$ of a set wrenches is denoted by (8):

$$\mathcal{M} = CH\left(\bigoplus_{i=1}^{n}\{\omega_i,\ldots,\omega_n\}\right) \text{ with } |f| = 1 \tag{8}$$

Where each contact wrench ω_i is generated by a unit force *f*. The set $\mathcal{U}$ is constructed by taking the union of a set of wrenches, denoted by (9):

$$\mathcal{U} = CH\left(\bigcup_{i=1}^{n}\{\omega_i,\ldots,\omega_i\}\right) \text{ with } \sum_{i=1}^{n}|f_i| = 1 \tag{9}$$

In this case, the magnitude f_i per contact is not constrained, but rather the sum of the contact forces. An important aspect of a hull is whether it is *positively spanning* its wrench space. This means that for any wrench in $\mathbb{R}^n$ space, a *positive* combination of α_{ij} can be found to counteract this wrench, which means that the given configuration is capable of resisting disturbance forces in all directions. This functions as a measure of stability in RG. A 2d example is given in figure 3.

2.5. definitions

Regarding convex hull operations, 3 wrench spaces form the basis for the majority of measures. Their definitions are given below.

2.5.1. Grasp wrench space. The mostly discussed wrench space is known as the *grasp wrench space* (GWS), which represents the potential forces and moments in all dimensions that a given configuration can generate assuming a predetermined force magnitude on the contacts. It is calculated by taking the convex hull of the *G* matrix implementing Minkowski sum addition.

2.5.2. Task wrench space. The task wrench space (TWS) represents the space of wrenches that are expected to disturb the system at hand. It is calculated by taking the Minkowski sum of the expected disturbance wrenches. It is stated as difficult to compute [56, 57], and measures based on this space are not discussed in this paper.

2.5.3. Object wrench space. The most general applicable wrench space is the object wrench space (OWS), which is comprised of all the wrenches that can be generated by sweeping a unit magnitude force across the boundaries of an object. It can be calculated by taking the union of all the wrenches that have been loaded on the object, where only the wrenches on the edges are sufficient to model the whole space accurately [58].

Next to these 3 definitions, there are 2 key definitions often used in RG literature. These have been interchangeably used however, where there is an important distinction to be made. In this paper, we adopt the definitions of Bicchi [59].

2.5.4. Form closure. Being one of the 2 key definitions of RG theory (sometimes also named total constraint), form closure is a purely geometrical property of a grasp. Forces play no role in determining whether a certain grasp is form closed or not.

In words, form closure states that for any motion in Euclidean $\mathbb{R}^n$ space, at least 1 constraint is violated if an object is to be form closed.

Mathematically it can be described as follows.

definition:

Let $\mathbf{n_i}$ be the normal vector of the object closest in the vicinity of contact point C_i, then the vector h_i is given by,

$$h_i = \left[-\mathbf{n}_i^T, (\mathbf{n}_i \times \mathbf{x}_i)^T\right] \tag{10}$$

The object is said to be *totally constrained*, when there is no admissible virtual displacement, such that;

$$\delta\mathbf{q} \text{ s.t. } \mathbf{h_i}\delta\mathbf{q} \geqq \mathbf{0} \quad \text{for} \quad \forall i \in [1, n] \tag{11}$$

2.5.5. Force closure. The second definition is called *force closure*. For a grasp to be considered force closed it should hold that for any external load, a reaction force can be generated by the grasp by a *non-negative* summation of primitive wrenches (in wrench space) or equally by a non-negative combination of forces exerted at the point contacts. It is said that the set of possible wrenches then 'exhausts' all of wrench space. Sometimes it is also referred to as a grasp 'positively spanning' the space of the system, although this is also considered true for form closure and thus leaves room for ambiguity. **definition:**

A system of n wrenches $\omega 1,...,\omega_n$ is said to achieve force closure when the space spanned by the corresponding wrench set $\mathcal{W}$, generated by the contacts is equal to R^k, which denotes the dimensional space of the object.

$$\mathcal{W} = \sum_{i=1}^{n}\xi_i\mathbf{w}_i : \xi_i \geq 0, \textit{ for } i = 1\ldots n \tag{12}$$

To compare both states, a grasp that is form closed is also always force closed. The other way around, only frictionless point contacts (FPCs) from force closed grasps can also be considered form closed, making form closure a more strict condition and a subset of force closure.

3. Selection

Given that there is an abundance of measures available from RG literature, a selection was made based on criteria that are stated in this section. This resulting selection of measures will be further discussed in the coming sections. Some criteria have been adopted or inspired from earlier review work [48, 52]. The list of criteria is as follows:

1) 2D and 3D suitable
2) Generally applicable
3) Independent on information regarding:
    a) Loading condition
    b) Manipulator constraints
    c) Object properties
4) Applicable with/without friction
5) Literature impact

The criterion of general applicability aims to filter out measures that are only suited for a specific situation or gripper. For clarification of performance metrics based on wrenches, only 2d wrenches are used, since these are based on 3 dimensional vectors and can thus be visualized. Most real world applications will however require a measure to be applicable in 3d, which results in 6 dimensional vectors that cannot be visualized. It has also been chosen to utilize measures that can potentially be implemented in a model with friction. Given that point contacts are considered, friction is assumed to be negligible in this paper. Lastly, the literature impact of the measures has been taken into account during selection. Next to these criteria, we propose to sort the resulting set of measures based on the following 2 categories, where category 1 is lend from [37];

1) Algebraic versus geometric measures
2) System level versus weakest link measures

Geometric measures refer to measures based on convex hull analysis, algebraic measures form the remaining group. System level versus weakest link refers to the focus of a measure, whether it is purely aimed at finding a weak spot, or more generally aimed at quantifying aspects of a grasp as a whole. The resulting selection consists of 6 measures, whom have been selected such that each category is represented; An exception to the criteria is the newly suggested least square method, which utilizes the reduced row echelon form in a different manner.

4. Measures

In this section, a more thorough analysis of the mentioned measures from section 3 is made. The 6 measures that will be explained further are;

1) The singular value decomposition
2) Least squares measure
3) Least resistant wrench measure
4) Object grasp wrench space measure

4.1. singular value decomposition

The first quality measures are based on the singular values of the G matrix. These singular values are obtained by performing a singular value decomposition (svd), which is applied on the covariance matrix of the grasp matrix seen in (13).

$$Mcovariance = G^T G \tag{13}$$

By calculating the covariance matrix (13), matrix G is made symmetric. The square root of the eigenvalues of the covariance matrix can then be calculated and will represent the singular values of G.
When considering a matrix as a linear transformation of Euclidean space, the svd subdivides this transformation into a rotation and a stretching operation [60]. During this subdivision, a new orthogonal system is calculated that represents the axis along which the transformation is *maximal*. The singular values σ_i that arise for each of the new axis represent the stretch along this direction. The svd is often visualized as an ellipsoid for 3 dimensional problems, where the singular values indicate the stretching along the primal axis of the ellipsoid.

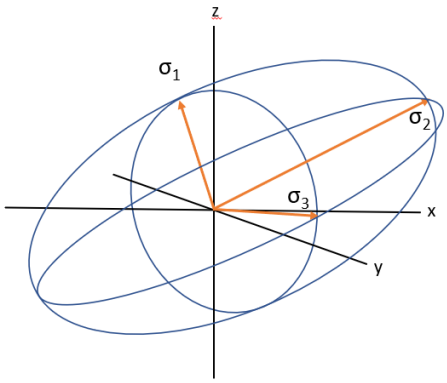

Figure 4: *Ellipsoid visualization of singular values*

This is depicted in figure 4. Important to note from this figure is that the new orthogonal system along which the singular values lie, does not correspond to the original axis system along which the matrix is build up. As a consequence, a singular value does not correspond one-on-one with a particular force or moment component. This has an impact on the extend to which a singular value is dependent on the placement of the origin. The force components of a wrench matrix are always origin independent. The moments, due to their selected origin of the moment arms, are not. Therefore, the placement of the origin impacts the magnitude of the moment component of the wrenches, which in turn impacts the shape of the ellipsoid and thus the relative magnitude of the singular values. By having an impact on the relative magnitudes of the singular values, the origin placement also has the ability to alter the scoring of some of the measures below.

The svd decomposition lies at the heart of the following 3 measures that have been suggested to use as an indication of the quality of a grasp [21, 55]. The measures are calculated by taking the svd of the *G* matrix.

4.1.1. Minimal singular value. The first suggested measure is to look at the smallest singular value (14). When a singular value approaches zero, the analysed matrix is said to 'lose rank'. This happens when 2 rows or columns become dependent on one another. It is described as the collapsing of the dependent dimension on the remaining ones, rendering a force or moment unconstrained. Generally, the Q_{msv} value is linked to a force DOF, given that moments are generally larger scalars due to the unit difference. Forces are also independent of origin placement given that their magnitude is not dependent on a moment arm, which renders this measure more or less origin independent. The impact of rotation of the new coordinate system does determine the level of origin dependency of the smallest singular value. If it is rotated more towards the moment axis of the original system, this dependency does increase. Maximizing the smallest value is suggested as a quantitative measure to maximize the robustness of a grasp. Because of the focus on the smallest singular value, this measures is categorized as a weakest link type.

$$Q_{msv} = \sigma_{min}(G) \tag{14}$$

4.1.2. Grasp isotropy index. Another suggestion is to look at the ratio's between the smallest and largest singular value (15). A more equal distribution arguably results in a configuration that is better resistant to unknown disturbances in all directions. The ratio will nearly always consist of singular values that are linked to a moment DOF and a force DOF, given that they have different units and thus different scaling. Although this link is dependent on the rotation of the new orthogonal system, it is often seen that there is a clear correlation between singular value behaviour and a specific DOF. Due to the comparison between a force related singular value and a moment related singular value, shifts in origin significantly impact this measure. The focus on overall performance makes this a system level measure.

$$Q_{gii} = \frac{\sigma_{min}}{\sigma_{max}} \tag{15}$$

4.1.3. Volumetric index. The third measure suggested from literature is the volume of the parallellepiped (16), also known as the determinant of the covariance matrix. This value is calculated by multiplying all singular values, or calculating the determint of the *G*. Utilizing all singular values makes this measure origin independent, despite the change in shape of the ellipsoid when the origin is displaced.
Larger singular values translate to a larger volume. Only the moment component of a wrench is sensitive to the displacement of a contact, the magnitude of the forces remains the same. As a consequence, increasing the volume is directly related to the size of the moments arms. This measure can therefore be used to maximize moment arms and thus provides information on a system level.

$$Q_{vol} = \sqrt{det(G^T G)} \tag{16}$$

$$Q_{vol} = \sigma_1 \cdot \sigma_2 \ldots \sigma_n \tag{17}$$

4.2. Reduced row echelon form

The *reduced row echelon form* [61], although not a measure on itself, can be an important tool in the analysis of constraint systems. The reduced form of the *G* matrix from fig 5 can be seen in eq (18). This matrix is a result from the applied Gaussian elimination surrounding the pivot points, where only row operations have been applied to calculate the reduced form. We know from Strang that the null space of the column space is preserved during these operations [60]. By putting the matrix in the reduced form, the 4th column will show the magnitude of the contacts in order to compensate for the 4th nesting contact, scaled to unit magnitude.

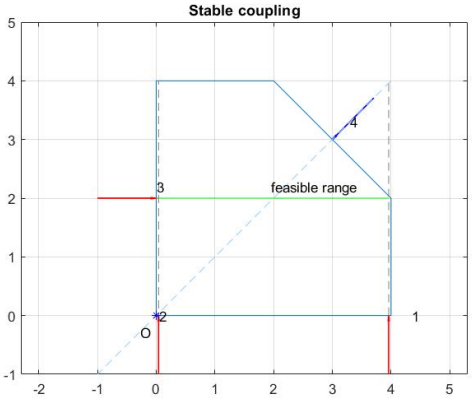

Figure 5: *Optimal configuration*

As a check, it can be observed that the 4th column represents the null space solution of the *G* matrix (19). Calculating this measure can thus be based on using either the reduced row echelon form, or by calculating the null-space, which requires an extra scaling step.

$$G_{reduced} = \begin{bmatrix} 1 & 0 & 0 & -0.354 \\ 0 & 1 & 0 & -0.354 \\ 0 & 0 & 1 & -0.707 \end{bmatrix} \tag{18}$$

$$[G]x = 0 \tag{19}$$

By looking at the signs of the null-space solution, one can determine whether a contact needs to push or pull in order for the system to maintain balance. Taking the reduced row echelon form of a matrix is thus a first method to determine stability of a configuration. It does however, only apply to exact constraint designs, and cannot be used for any other number of constraints.

4.2.1. Least squares measure. This newly suggested least squares measure (Q_{lsm}) is based on the magnitudes of the equilibrium solution. In case disturbance- or loading forces on a newly designed coupling are not known, one would tend to go for an all-round performing coupling, where the loading amongst the contacts is pushed to equal distribution during the design phase. Given that the nesting force needs to be counteracted by the contacts, the loading ratio for each contact can be calculated (20) which would represent the most equal distribution.

$$f_i = \frac{1}{\sqrt{n}} \tag{20}$$

Here, n represents the number of contacts. F_i represents the desired magnitude per individual contact.

$$ft = \sqrt{(f_1)^2 + ... + (f_n)^2}, \tag{21}$$

F_i can then be used to calculate Ft, which represents the resulting counter force for the nesting force, and should thus have equal norm and opposite direction. The errors between the optimal magnitude (f_i) of a force (20), and the actual magnitudes of the contacts x_i, calculated using equation (19), are then subtracted from one another. The total error is calculated in a least squares manner, where it is first squared and then summed and divided by the amount of contacts (22). Due to the focus on overall distribution of forces, this is a system level measure.

$$Q_{lsm} = \frac{1}{n}\sum_{i=1}^{n}(f_i - x_i)^2 \tag{22}$$

4.3. Geometric methods

Geometric measures is a category that incorporates all the measures based on convex hulls. In literature this represents the mostly discussed category of measures, where the 3 basic wrench spaces mentioned in chapter 2.4 form the basis for the majority of the measures.

4.3.1. Least resistant wrench (Q_{lrw}). The least resistant wrench, already mentioned in section 1, is the most discussed measure from RG. It is based on the G matrix, where it represents the distance between the origin and the closest facet of the GWS. The GWS represents the convex hull which is calculated by taking the Minkowski sum of G. Figure 6 shows a randomly selected configuration, with the corresponding G matrix shown in (23). The convex hull of this matrix is depicted in figure 7. The arrow indicates the closest facet towards the origin. Either the norm of the arrow is taken as measure, in which case it is known as the *largest inscribed sphere*, or the inverse of the coordinates on the facet are taken as the direction in which disturbances are hardest to resist. In this case it is called the *least resistant wrench*. As long as the distance between the closest facet and the origin is larger than zero, a configuration is able to generate forces and moments in all directions, proving at least marginal stability and a positive span of that particular configuration.

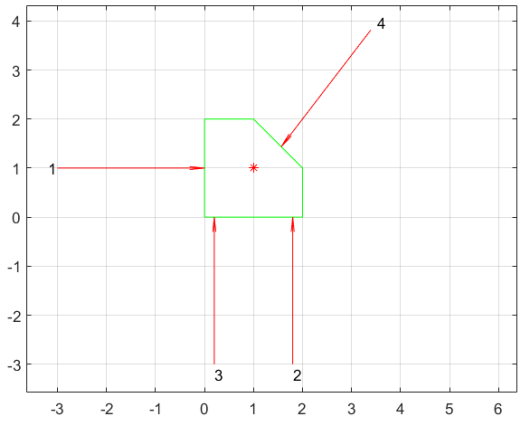

Figure 6: *Stable coupling*

$$G = \begin{bmatrix} 1 & 0 & 0 & -0.609 \\ 0 & 1 & 1 & -0.794 \\ 1 & -0.2 & -1.8 & 0 \end{bmatrix} \tag{23}$$

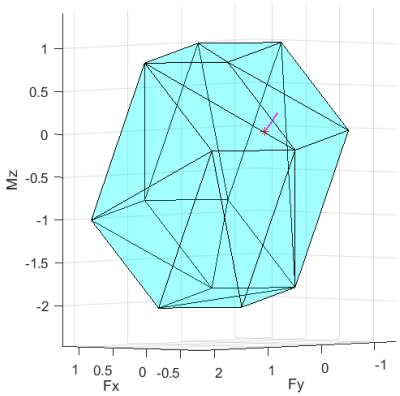

Figure 7: *CH(G) with arrow indicating closest facet*

The found least resistant wrench does not necessarily represent an existing unit wrench however. In some cases when modelling the found wrench as a unit force on the object which generates a moment around the origin, the line of action of the force does not intersect the geometry, which makes the physical meaning of this measure somewhat obscure.
Next to this, the shape of the hull, and thus the measure itself is significantly affected by origin displacement. Origin dependency is a problem in all measures based on convex hull operations. Over the years, there have been multiple suggestions to cope with this problem [33, 48, 58, 62]. The suggestion considered best will be discussed next.

4.4. Combined space methods

There is one promising suggestion from literature to overcome the origin dependency without losing quality of information. The suggested measure is the scale factor

between 2 hulls that are combined [56]. For example, the minimal scale factor between the *Object Wrench Space* (OWS), introduced in section 2.4, and the GWS. The minimal scale factor that scales the OWS such that it is completely enclosed GWS, determines exactly which wrench is the hardest for the GWS to resist. The OWS is generally calculated by 'loading' the edges of the object with unit disturbance forces, depicted in figure 8, whom are combined into the OWS hull by means of applying union sum addition.

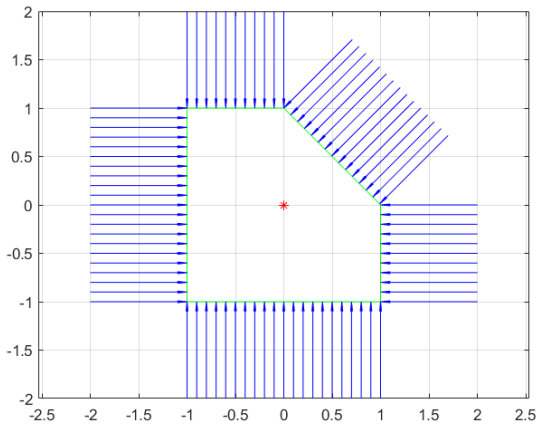

Figure 8: *Disturbance vectors on object*

The vectors of the point contacts are then combined into the GWS by Minkowski sum addition. This way, the magnitude of the contacts is summed, which represents the cooperation of multiple contacts to withstand a single disturbance force. The scale factors can be calculated by solving the optimization problem depicted in (24) for each of the vertices of the OWS, denoted by V_{ows}. Here, x and y are optimization variables. Variable y returns the scale factor required in order to contain the particular vertex within the GWS [63].

$$\begin{aligned} \min_{f} \quad & f = -(y + \sum x), \\ \text{s.t.} \quad & V_{ows} \cdot y - G_{gws} \cdot x == 0 \\ & 0 \geq x \geq 1 \\ & y \geq 0 \end{aligned} \tag{24}$$

The smallest scale factor y is used as measure, from now on referred to as the Q_{og} measure (25).

$$Q_{og} = \min(y) \tag{25}$$

Given that the 2D wrenches are 3D mathematical entities, the scaling can be visualized, seen in figures 9 and 10. The arrow indicates the direction of the smallest scale factor in order for the OWS (scaled hull) to be complete enclosed within the GWS.

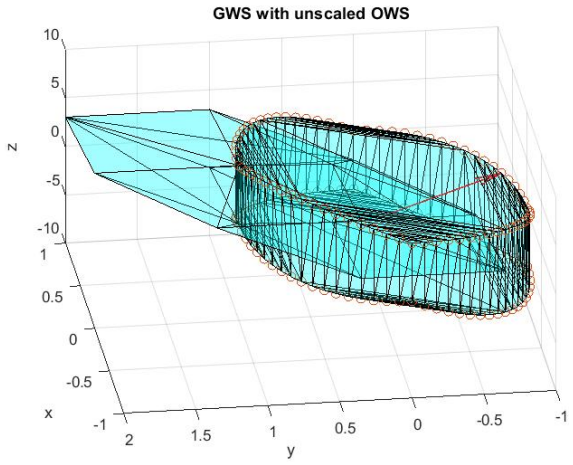

Figure 9: *Unscaled OWS, too large forces to be contained by the GWS*

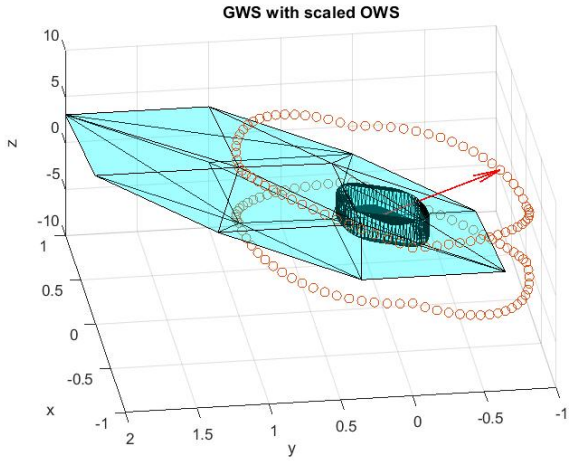

Figure 10: *Scaled OWS, with indicator for weakest direction*

This measure can be particularly useful when designing for overall optimal performing couplings. Because the ratio is taken between these 2 hulls, the origin dependency problem is solved whilst still maintaining the quality of information. This is the only measure with both these traits. It is considered an improved version of the least resistant wrench method, where complexity is increased as a trade-off for a more general applicable method. This increase in complexity is generally manageable in 2 dimensions. In the 3d case however, computational efficiency generally becomes an important topic. The same trick of hull combination can be applied to any combination or estimate of wrench spaces. When one is considering more task specific designs for example, the TWS, which is the wrench space comprised of all expected disturbance wrenches [56, 57], can also be used instead of the OWS.

5. Implementation

In this section, some choices in contact modeling are discussed, as well as how the measures are implemented in this main case study. This case study is performed in order to analyse the behaviour of the measures when implemented for coupling design. After this clarification, it will be discussed how the starting data set and the results from section 6 were obtained.

5.1. bilateral vs unilateral

The important distinction between bilateral and unilateral contacts has already been discussed in chapter 1. In robotic grasping, all measures are implemented in a unilateral manner. In order to implement RG measures on coupling design, the nesting force can no longer be assumed to be a force with undefined magnitude or origin. It will be modelled as a point contact. This is required, given that the half space span of the remaining contacts would mean that a convex hull would never be of 'full span', explained in chapter 2.5, which would render any hull based method unusable. Not all measures of RG are implemented in a unilateral manner however. What becomes obvious from the work of Strang [60], is that the svd is of bilateral nature, something not yet discussed in chapter 4. A so called sign ambiguity during this composition makes that this measure cannot distinguish the impact of positive versus negative vectors [64]. This is depicted in figures 11 and 12, where the flipping in sign of the wrench generated by contact 4 has no effect on the singular values. As a consequence, this measure on its own is not capable of predicting stability.

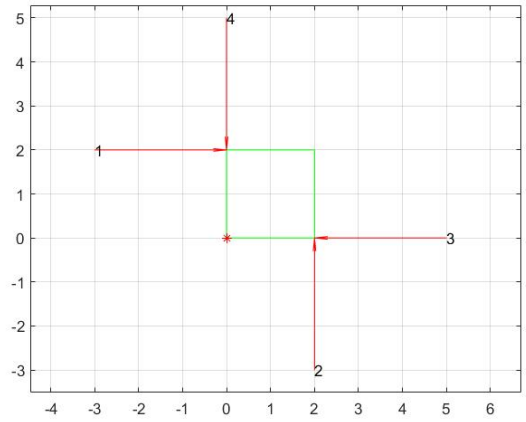

Figure 11: $\sigma_1 = 2, \sigma_2 = \sqrt{(2)}, \sigma_3 = \sqrt{(2)}$

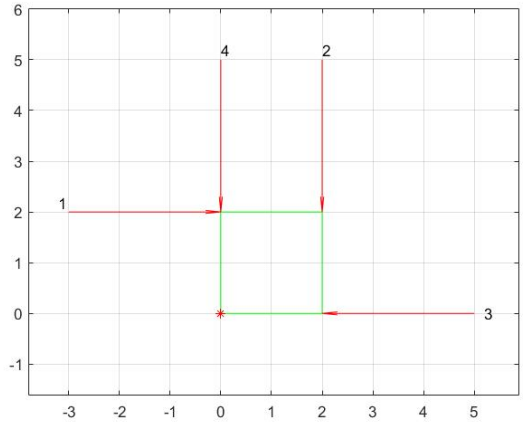

Figure 12: $\sigma_1 = 2, \sigma_2 = \sqrt{(2)}, \sigma_3 = \sqrt{(2)}$

This sign ambiguity makes that this measure would be more suitable for a bilateral constraint analysis. For this reason it has been chosen to split up the implementation of the svd based measures, and follow the coupling methodology through the assumption of bilateral contacts. As a result of this approach, the svd based measures are implemented on the point contacts only, not on the nesting force contact. In a second step, the optimal position of the last contact should then be determined through the implementation of a different measure.

As a consequence of this approach, the quality of the full configuration is not rated by the implemented svd measure. Next to this, both orientation and location of the fourth contact needs to be determined. Usually in coupling design, the nesting force is simply an inverted sum of all the local forces. This approach does not offer a suggested location for the nesting force however, since only forces and not moments are considered. Therefore, a small subsection in chapter 6 is dedicated to the results of combining the volume measure of the svd with the Q_{lsm} measure. These measures have been selected given their origin independency, which gives them a distinct advantage over other measures. In order to get an idea of the quality of these results, it has been chosen to experimentally verify the correctness of the Q_{og} measure described in chapter 4.4. After verifying the physical correctness of the calculated scale factors, this measure will be used as a benchmark.

5.2. Performance study

In this section it will be first explained how the main performance study is conducted, that analyses the overall traits per measure when implemented on coupling design. The object that is chosen to be coupled can be seen in figure 13. It has been selected because the best coupling configuration for this block has already been geometrically deduced [65], this knowledge will be used to verify the performance of the measures.

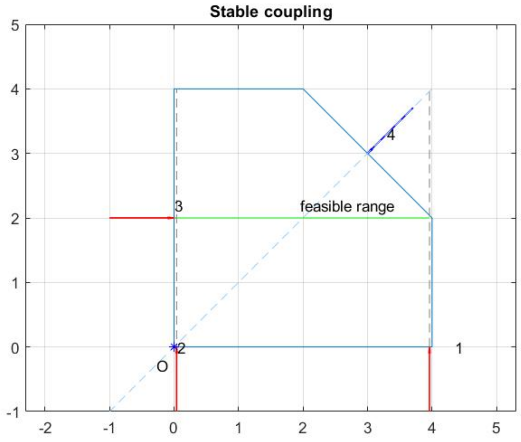

Figure 13: *Optimal coupling*

It is considered the most optimal case, although a multitude of optimal configurations does exist, as long as the nesting force intersects the feasible range in the center. A large set of *potential* stable configuration has been generated by applying vectors all around the object, seen in figure 14. A predetermined coupling direction, depicted by the red arrow, has been used to filter out unwanted potential contact vectors. The contacts are constrained to the tangent and opposing half-space of the predetermined coupling direction. This way, freedom of coupling is guaranteed.

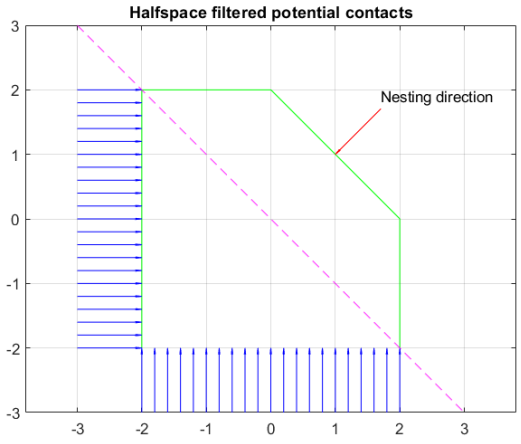

Figure 14: *potential contacts*

The same method has been applied to a larger data set where the contact vectors were also applied under angle, which represents all the potential nesting force vectors. The remaining set after the half-space filtering can be seen in figure 15.

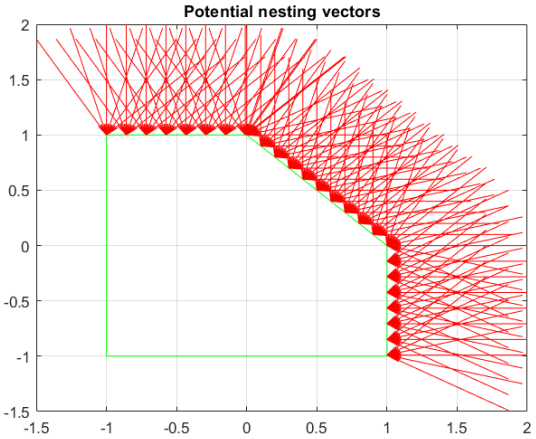

Figure 15: *potential nesting forces*

All possible combinations of 4 vectors are generated with these 2 sub-sets. Before implementation, the configurations are first filtered on stability by means of implementing the suggested row reduced form sign check, discussed in section 4. For the bilateral approach, the contacts from the first set are sorted in all possible 3 contact combinations, whom are tested by Q_{vol} first. After this, the configurations are combined with a 4th contact and scored by Q_{lsm}. This scoring will select the best configuration.
Unlike this bilateral approach, the unilateral approach consists of only scoring the stable configurations comprising of all 4 contacts. The separate step of scoring the 3 point contact combinations can be omitted in this analysis.

The results of both approaches will be next discussed in chapter 6.

6. Performance study results

The results of implementing the selected measures on a generic object that needs to be coupled will be shown in this section. The algebraic results are presented first. It is important to realise that the chosen object in this case study is symmetric and the origin has been placed in the center. This has been done to simplify the situation which better visualizes the different properties of measures.

6.1. Algebraic measures

The figures that are used in this chapter to clarify the effects of different measures have been partly included in Appendix A.

6.1.1. svd measures. Figures A.1.1a - A.1.2b show the effect of the Q_{msv} measure that is only focused on the weakest link. Firstly, figures A.1.1a and A.1.1b show configurations with equal rating, though whilst the Q_{msv} value remains unchanged, the decreasing moment arm has a negative influence on configuration A.1.1b. Figures A.1.2a and A.1.2b are included to show that the Q_{msv} value can shift from representing forces to representing moments depending on the size of the moment arms which determines the smallest singular value. Displacing the bottom contact

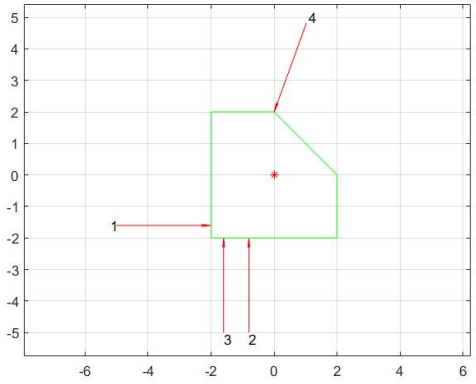

Figure 16: Q_{lsm} *first option*

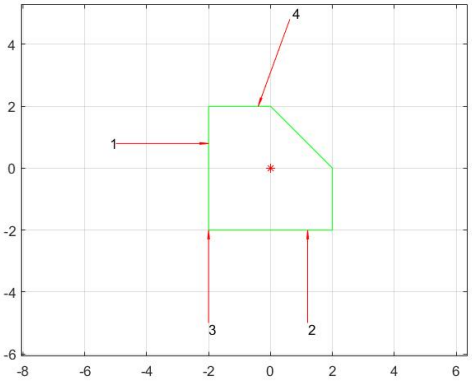

Figure 17: Q_{lsm} *second option*

has no impact on the measure. The measure can be more or less sensitive to a change in origin depending on whether the smallest singular value is linked to a force or a moment. In the latter case it will have a larger effect, though to what extent is purely depending on the rotation of the orthogonal system, which is discussed in 9.
The Q_{gii} measure does not provide a single optimal configuration, but rather a set of configurations. The extrema of the 2d case set are depicted in figures A.1.3a and A.1.3b. Because the third singular value is not incorporated in the calculation of this measure, it can float in between σ_1 and σ_2 without influencing this measure, showing again the downside of not taking all measures into account.
The last svd based measure to be implemented is the volume measure. The moment arms are maximized through the use of this measure. The position of force vector 3 has no effect on the magnitude of this measure, which can be explained by the fact that this vector generates a force only which has no effect on the determinant. Figures A.1.4a and A.1.4b show the extreme cases where vector 3 can shift along its vertex without changing the Q_{vol} scoring.

6.1.2. Least squares measure. Figures 16 and 17 both show 2 out of many optimal configurations, where all optimal configurations share a fourth nesting contact intersecting the feasible area exactly in the middle. This way, forces generated to counteract moments are balanced and thus provide the least error. The figures show that the measure is only sensitive to the relative magnitude of the contact forces. The generated moments through these contacts are not taken into account.

6.2. Geometric measures

In this section, the least resistant wrench method and the verified Q_{og} measure will be discussed.

6.2.1. Least resistant wrench. Again for clarification, the first example to be discussed will be the optimal configuration regarding a 2d cube, where perfect symmetry makes the behaviour of the measure easier to interpret.
Figure A.2.1a shows the grasp which will be analysed first. The depicted grasp has been selected by the least resistant wrench measure, where all possible grasps consisting of 4 contacts angled from -45 degrees to 45 degrees on the object have been tested. The forces are equally distributed and generate equal and opposite wrenches, which results in the symmetric hull from figure A.2.1b. The drawn arrows indicate the point on the hull which is closest to the origin. Given that all facets are equally distanced from the origin, this grasp is considered optimal. The object has been increased in scaling to allow for larger moment arms between the contact vectors. The effect can be seen in figure A.2.1c, where the distance towards the origin has increased through the more upright position of the facets.
The next figures have been generated by scoring the same data set as the algebraic measures with Q_{lrw}. The configuration with the optimal contact placement according to the Q_{lrw} measure is depicted in figure A.2.2a. The corresponding hull is depicted in figure A.2.2b, where the typical tetrahedron shape is now tilted in orientation.
An important aspect regarding this measure is that it is purely focused on the direction with the smallest wrench, or the position where the inscribed sphere first touches the hull. The changes in other facets are not considered as long as their distance with respect to the origin is larger. An example is given in figure A.2.2c, which can be compared with figure A.2.2a. The shift in position of contact 2 has no effect on the distance towards the closest facet, and is still scored as equally optimal. The coupling has been scaled to enhance the effect.
The last important aspect of the Q_{lrw} measure is the origin dependency problem. The configuration in figure A.2.3a has a displaced origin, which severely affects the performance of this measure. The imbalance caused by this displacement can be best visualized by inspecting the shape of the hull, depicted in figure A.2.3b. One can see that the wrench with negative moment is very small, and causes a large change in shape. There is also a change in contact placement due to this deformation of the hull.

6.2.2. Object grasp wrench space measure. The last results are generated by implementing the grasp wrench space measure from section 4.4. Figures A.2.4a and A.2.4b show the range of results that have an equal measurement scoring. One can see that the instantaneous center

of rotation of contact 1 and 4 is placed in the center between contacts 2 and 3, which balances the moment arms of the bottom contacts and thus results in an optimal resistance in either direction. Figure A.2.4c also shows the unit disturbance forces (in purple) that generate wrenches which are hardest to resist for this particular configuration. The scale factor for both of these wrenches is 0.354, which means that for a unit disturbance force to be resisted, the contacts would have to apply roughly 3 times that force on the contacts to generate a sufficient counter force.

6.3. Experimental results

Like mentioned in chapter 5, the physical information retrieved by applying the Q_{og} measure was experimentally verified before it was implemented as a benchmark. A setup was build where the magnitude of the disturbance force could be determined, that would render the configuration from figure 18 unstable.

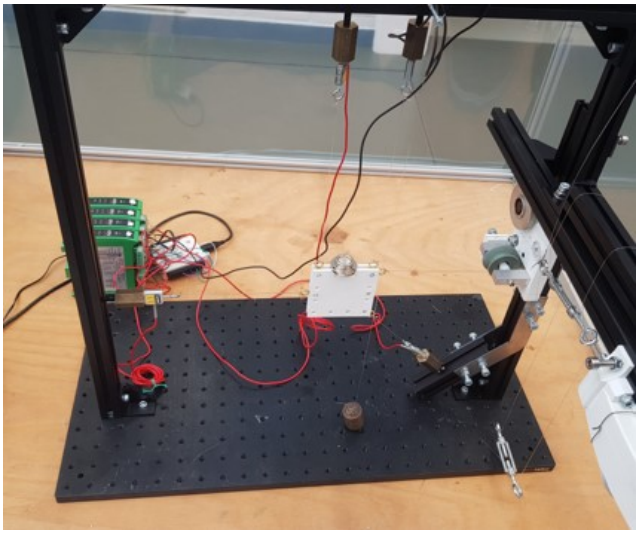

Figure 18: *Experimental set up*

Figure 19 shows how the forces are shifted along their lines of action in order to go from a configuration with compressive forces towards a tensile configuration.

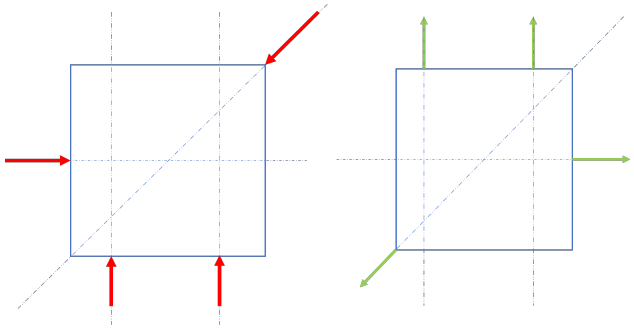

Figure 19: *Compressive forces (L) Tensile forces (R)*

This way, tensile force sensors could measure the forces in the suspending cables. Another important benefit is that slippage of contacts and friction play no role in the results in this set up. Figure 20 (L) shows a schematic of how a disturbance force is applied on the coupling, (R) shows a simplified version of the corresponding convex hull of this configuration, where the moments have been left out for clarity. The red dot indicates the magnitude at which the disturbance force becomes too large for the contacts to compensate. A live reading of the tensile forces in the cables whilst the magnitude of the disturbance force was increased, showed a contact force reaching zero at this point, which indicates the tipping point of a configuration becoming unstable.

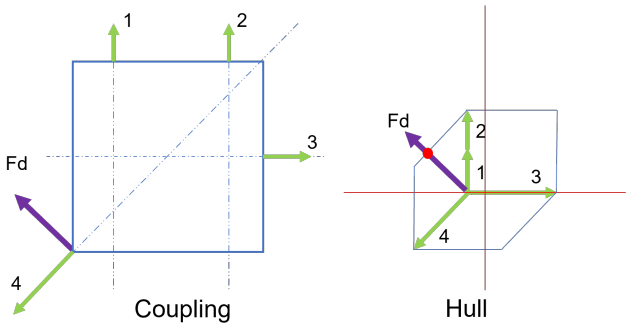

Figure 20: *Representation of the effect of a disturbance force on the hull*

Both the magnitudes of the pre-loading forces and the position and the angle of the disturbance force has been altered throughout multiple tests. The results of the measurements are depicted in figure 21.

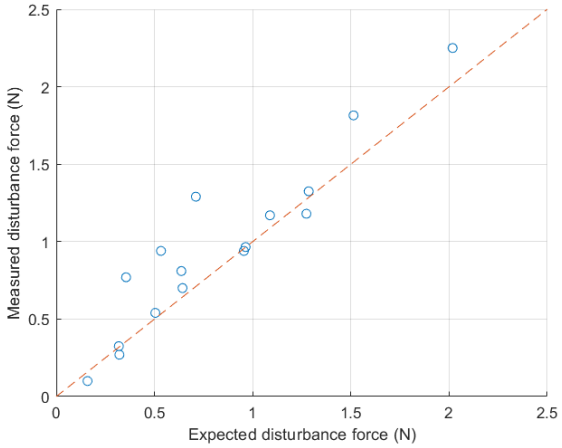

Figure 21: *measured vs expected magnitude of unbalancing disturbance force*

A more elaborate explanation of the experiment is given in Appendix B.3.

7. Case study results

Like mentioned in section 5, this section provides the results of comparing the Q_{og} measure with the suggested combination of Q_{lsm} and Q_{vol}, indicated as Q_{comb} in table 1. Both measures been implemented on 5 shapes that have been randomly generated, each with 1 optimal

configuration according to the Q_{og} measure. Table 1 shows the scoring of the measures relative to one another. The first column indicates the amount of configurations that the Q_{og} measure has processed. The combined measure however, processes the contacts and the nesting force options separately. For example; set 1 has a total of 12.766 options that are all considered and scored by the Q_{og} measure. For the combined measure however, the pre-selection step where only 3 contacts are scored in a bilateral manner, already discards approximately 10.000 options. This partly explains the significantly reduced computation time.
The Q_{og} score gives the value of the best found configuration. The Q_{comb} scoring then shows the Q_{og} score of the configuration that this measure picked as best resulting. The percentage score indicates the amount of configurations that scored better on the Q_{og} scale compared to the configuration which scored the highest by Q_{og}. The last two columns indicate the computation time it took to process the initial data set.

Set nr	Set size	Scoring			Comp. time (sec)	
		Q_{og}	Q_{comb}	Percentage	Q_{og}	Q_{comb}
1	12.766	0.567	0.472	0.49%	76.14	0.15
2	12.396	0.452	0.452	0.14%	76.07	0.33
3	24.074	0.590	0.520	0.16%	182.76	0.53
4	18.096	0.676	0.541	5.79%	136.38	0.32
5	65.720	0.615	0.533	0.63%	518.69	2.21

TABLE 1: *Performance of combined measure*

8. Overall results

8.1. Performance table

Figure 22 provides an overview of the important aspects per measure, and how these are scored relative to one another. An important distinction between measures is the system level (SL) versus weakest link (WL) type of measures, which is depicted in the first column.
The physical interpretation score is a heuristic score, where the number 2 is given to measures that provide clear information that can be interpreted 1 on 1 with a physical aspect. A zero score on the other hand, means that the information received by applying this measure does not quantify a physical aspect in any way. Q_{lrw} receives a scoring of 1. This is because the found wrench represents a physical entity, though the wrench can be distorted by displacement of the origin. Generality refers to whether or not a measure can be implemented on different objects and still be compared relative to one another. This is usually depending on whether the measure is origin independent or not. Lastly it is important to mention that the complexity of the Q_{og} measure is assumed to be similar to the Q_{lrw} measure. Both the OWS and GWS convex hulls are required for this measure, whom can be calculated by implementing the Quickhull algorithm. Of both hulls, the OWS is generally comprised of significantly more wrenches and therefore this calculation step dominates overall computation time of the Q_{og} measure. However, the OWS does not change when different configurations are being tested on the same object. Therefore, the points that make up the convex hull only need to be calculated once, after which this data can simply be passed on for the next configuration to be scored. The impact of this approach on computation time is visualized in figures 24 and 25.

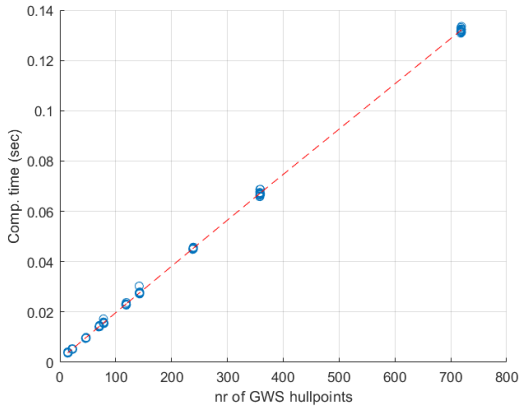

Figure 24: Q_{og} *comp. time with precalculated OWS*

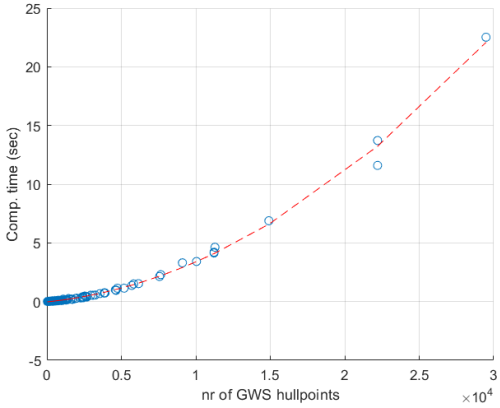

Figure 25: Q_{og} *full comp. time*

8.2. Flowchart

In order to provide a detailed plan regarding when to implement which measure and in what way, a flowchart has been constructed, seen in figure 23. It is meant to serve as a first guideline for the design of couplings out of a larger set of configurations. The flowchart is based on 4 core questions;

1) A: Is the data set small enough to be processed through Q_{og} analysis?
2) B: Is the configuration ECD?
3) C: Is the data checked for stability?
4) D: Is the coupled object symmetric?

The resulting flowchart offers options for any design scenario, though some scenario's offer better options than others. The first important question is whether the design will be exact constraint or not. Either the reduced form can be used for stability in an ECD case, which is significantly faster in terms of computation time than calculating the hull of a configuration, and checking whether the origin

	Type	Stability		Nr of wrenches		Physical interpretation		Object incorporation		Generality		Complexity		Scoring
Q_{lsm}	SL	Yes	1	ECD	0	Clear	2	No	0	Yes	1	Θ(m*n(min[m,n]))	3	7
Q_{gii}	SL	No	0	Unlim.	1	Abstract	0	No	0	No	0	Min([m,n])	3	4
Q_{vew}	SL	No	0	Unlim.	1	Abstract	0	No	0	Yes	1	Min([m,n])	3	5
Q_{msv}	WL	No	0	Unlim.	1	Abstract	0	No	0	No	0	Min([m,n])	3	4
Q_{lrw}	WL	Yes	1	Unlim.	1	Medium	1	No	0	No	0	O(n*log(n) - n^2)	2	5
Q_{og}	WL	Yes	1	Unlim.	1	Clear	2	Yes	1	Yes	1	graph	2	8

Figure 22: *Measurement scoring*

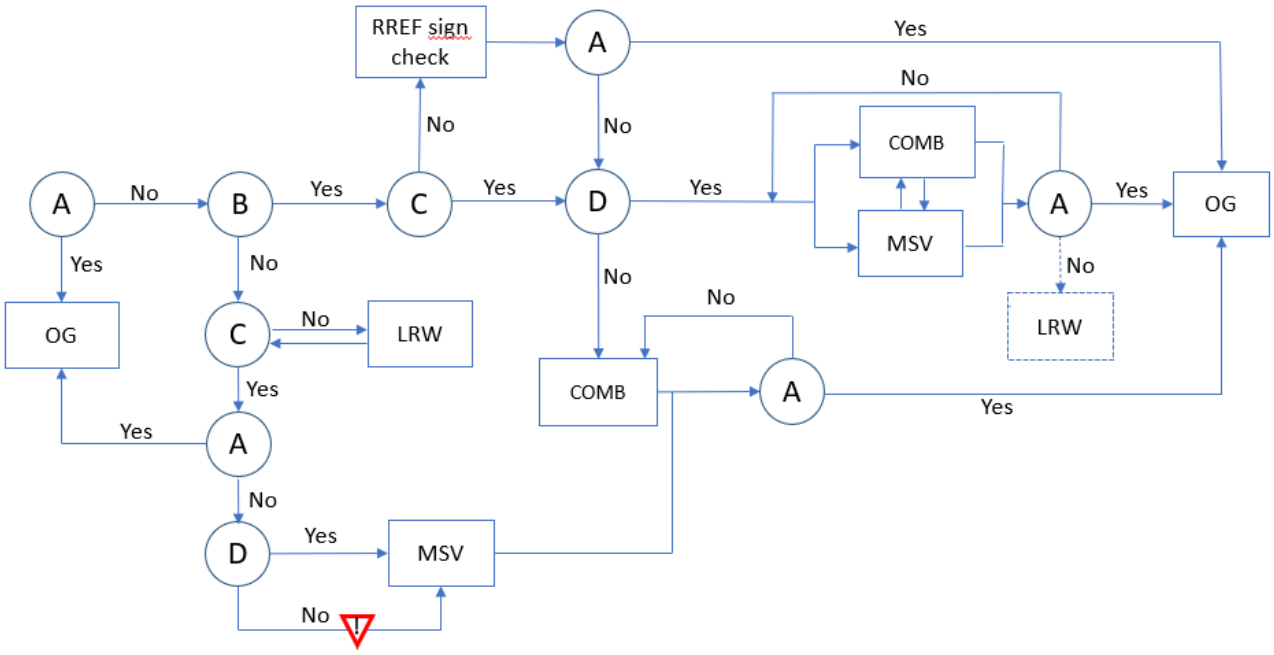

Figure 23: *Implementation flowchart*

is incorporated or not. This latter option is the alternative method for determining stability of a non-ECD configuration. Symmetry also plays an important role for the origin dependent measures. Given that the position of the origin generally has to be selected by the designer, it gives rise to uncertain results when the object is non-symmetric. A different position can lead to different results. In the case of a non-symmetric and non-ECD design, filtering a data set until it is small enough to be processed by the Q_{og} measure can only be done with svd based algebraic measures. Although computationally cheap, the results can be misleading, which explains the warning triangle sign. For couplings, non-ECD designs generally will not be a problem, which gives designers more options. When a design is both symmetric and exact constraint, one can choose the least resistant wrench method as final scoring measure as well, in case it takes too long to compute the OWS for example.

9. Discussion

9.1. Algebraic measure performance

9.1.1. svd. This decomposition is a generalization of a matrix, and is generally used for large data sets to look for

commonalities. For this application it is interesting to look at the 1-to-1 relation of a singular value versus the degrees of freedoms that are constrained. This relation however, becomes obscure due to the rotated coordinate system. In literature, little work has been found regarding the utility of the svd decomposition for more specific application on smaller matrices. For the Q_{msv} and Q_{gii} measure, more insight in the relation between the singular values and the degrees of freedom would help the implementability of these measures. Particularly the measures that suffer from origin dependency through the comparison of forces versus moments can benefit from a clear distinction in singular values and how to separate these 2.

9.1.2. Q_{lsm}**.** The Q_{lsm} is a computationally cheap measure that is easy to interpret. In the case of an ECD amount of contacts, the stability can be best checked by the reduced form sign check. The magnitude of the point contacts for equilibrium are calculated as a by-product. As a consequence, calculating the Q_{lsm} has little impact on computation time given that the required information is already at hand. The weak point of this measure is the assumption of equal distribution. In some cases the error can be minimal through the neglect of 1 contact point whilst the others are loaded in a near-optimal manner. Therefore, a minimum magnitude per contact can be implemented as a weakest-link type of constraint next to the calculation of the overall error of the contacts.

9.1.3. Q_{comb}**.** The Q_{vol} and Q_{lsm} measures complement each other, given that one is purely focused on a proper force distribution, whilst the other maximizes the moment arms. The computational benefit compared to geometric measures is significant. Particularly when considering the 3d scenario, where hull measures are generally calculated using computationally complex optimization programs. The method is implemented in the exact same manner for the 3d case, with the distinct benefit that it is relatively simple to implement compared to the hull measures, whom are considerably more complex in terms of both computation time as well as implementability. The Q_{comb} measure however, does show significant fluctuations in the results that are depicted in table 1. Configuration 4 shows a 5.79% decrease of Q_{og} scoring whilst the other configurations score significantly higher. It is to this point unclear what aspects of this configuration are the reason for this large deviation, which is important to investigate in future work in order to fully comprehend te limitations of the Q_{comb} measure.

9.2. Geometric measure performance

The least resistant wrench measure has been incorporated in this paper because it is so widely discussed in literature. An interesting feature that is not yet discussed is the impact of an estimated origin on the quality of the information. Most adaptations like characteristic length [33] or dimensional reduction [48], provide little extra meaning towards the eventual results. It has been noted from different non-symmetric objects that positioning the origin somewhere around the center does not generally have a significant impact on the relative value of the inscribed sphere, although this relation is hard to quantify.

A distinct benefit of the Q_{lrw} measure relative to the Q_{og} measure in particular is the computational efficiency. MATLAB has a ready-to-use command to calculate n-dimensional hulls using the Quickhull algorithm, which is still in the same range of computation time for 3 dimensions relative to 2 dimensions when considering the GWS. The OWS however, poses a problem when it needs to be calculated in 3 dimensions given the increase in computation time. The algorithm from [63] has already shown drastic increase of computation time in comparison to a 2d geometric approach of calculating the scale factors. The impact of computation time in 3d is an important aspect to be researched further, but the complexity of proposed algorithms made the comparison non-straightforward in terms of implementation on a general case.

9.3. General overview

The suggested flowchart from figure 22 is a first guideline for a new suggested approach methodology for designing new couplings. There are still various aspects that can be improved. In general, a bulk generated approach is not optimal, though when computation times are acceptable these algorithms are generally more easy to implement compared to iterative search methods for the best configurations. Also, often these iterative search methods do need a first initial configuration on which the search can continue. For these types of algorithms, the computationally cheap measures can quickly provide a viable starting configuration. An important step towards improving the flowchart would be to implement it in 3d scenario's and test the performance of the convex hull measures. Unfortunately, the optimized code of articles is often not shared , which motivated the choice to go for less optimized algorithms and compare performance in a more general manner, lesser focused on optimizing the computation time.
Like mentioned in chapter 1, the 2 primal aspects of designing a coupling are the loading condition and the error motions. Particularly the first aspect can be better analysed by making use of the RG theory that has been presented so far. Using the reduced form of the *G* matrix, or the scale factor between a TWS and the GWS can provide insight in expected loading conditions of a newly designed coupling. Last mentioned hull measures have the distinct advantage that more than just ECD designs can be analysed. This offers the potential to model the amount of overconstraintness of a configuration, which can be combined with better insight in local loading conditions for an optimal analysis of the deterministic dilemma of a design. The second main aspect of coupling design is the analysis of potential error motions. Some work has been done implementing screw theory in a more algebraic and virtual motion-like implementation [66–68]. By making use of the twists of a system, the extent to which a contact is penetrated per motion is analysed, which provides insight

in the effectivity of a contact to withstand a certain twist of the object. This could potentially be combined with the hertzian contact analysis that is often conducted in coupling literature.
Friction is another aspect that contributes significantly to error motions, particularly during loading of couplings. The modelling of higher order contacts (HOCs) is often done throughout RG literature and has the potential to be incorporated into a more advanced loading error analysis.

10. Conclusion

In this paper, the value of the quality measures from robotic grasping for the design process of kinematic couplings has been proven. This has been done by starting with a general selection of widely applicable measures with different aspects, representing a wide variety of available measures from literature. The differences in theory between these 2 fields have been elaborately discussed, after which a 2d performance study was conducted with a dual purpose. First and foremost, it had the goal of proving that the gap in implementation between these fields could be bridged. Second, this performance study had the purpose of visualizing the traits of each measure when implemented on a coupling design process and to allow these traits to be compared amongst the other measures. Up until now, no clear comparison was made in literature between RG measures, in order to get a feeling for relative performance.
Based on these results, it is suggested to combine 2 algebraic measures. Their combined performance is then compared relative to the Q_{og} measure, which is experimentally verified in order to be used as a benchmark for this new measure.

It can be concluded based on the results from the 2d case study, that indeed the gap between these fields is based on a difference in modelling, which can be bridged. By switching the bilateral and unilateral approach for certain measures and describing the design problem differently, a multitude of measures can be implemented in the design process for new kinematic couplings. These measures are a first method to give feedback on how well a new configuration for a coupling will perform. The combined hull measures provide the tools to model the loading stresses at the contacts when the system is disturbed. These stresses are important, because they constrain the loading of the coupling, which is a key factor in design of couplings.
Based on the results of the case studies performed along with gained insight during analysis, the flowchart in figure 22 has been constructed. It is intended to serve as a guideline in this new design process, concluding this work as a first step towards a more elaborate design methodology that will help increase the implementation of kinematic couplings in industrial applications.

References

[1] A. Slocum, "Kinematic couplings: A review of design principles and applications," *International Journal of Machine Tools and Manufacture*, vol. 50, no. 4, pp. 310–327, 2010, ISSN: 08906955. DOI: 10.1016/j.ijmachtools.2009.10.006. [Online]. Available: http://dx.doi.org/10.1016/j.ijmachtools.2009.10.006.

[2] E. Pearce, A. Parkinson, and K. Chase, "Tolerance analysis and design of nesting forces for exactly constrained mechanical assemblies," *Research in Engineering Design*, vol. 15, no. 3, pp. 182–191, 2004, ISSN: 09349839. DOI: 10.1007/s00163-004-0053-9.

[3] J. C. Maxwell, "General considerations concerning scientific apparatus," in *The Scientific Papers of James Clerk Maxwell* (Cambridge Library Collection - Physical Sciences), W. D. Niven, Ed., Cambridge Library Collection - Physical Sciences. Cambridge University Press, 2011, vol. 2, pp. 505–522. DOI: 10.1017/CBO9780511710377.053.

[4] J. Leidich, "Minimized converging single-point (MConS) kinematics: A novel approach to fastening detachable spacecraft structures," in *AIAA SPACE Conference and Exposition 2010*, American Institute of Aeronautics and Astronautics Inc., 2010, ISBN: 9781600869662. DOI: 10.2514/6.2010-8762.

[5] J. B. Taylor and J. F. Tu, "Precision X-Y microstage with maneuverable kinematic coupling mechanism," *Precision Engineering*, vol. 18, no. 2-3, pp. 85–94, 1996, ISSN: 01416359. DOI: 10.1016/0141-6359(96)00036-0.

[6] M. Russo, J. Barrientos-Diez, and D. Axinte, "A kinematic coupling mechanism with binary electromagnetic actuators for high-precision positioning," *IEEE/ASME Transactions on Mechatronics*, vol. 4435, no. c, 2021, ISSN: 1941014X. DOI: 10.1109/TMECH.2021.3074286.

[7] K. M. Varadarajan and M. L. Culpepper, "A dual-purpose positioner-fixture for precision six-axis positioning and precision fixturing. Part I. Modeling and design," *Precision Engineering*, vol. 31, no. 3, pp. 276–286, 2007, ISSN: 01416359. DOI: 10.1016/j.precisioneng.2006.11.002.

[8] R. R. Vallance, C. Morgan, and A. H. Slocum, "Precisely positioning pallets in multi-station assembly systems," *Precision Engineering*, vol. 28, no. 2, pp. 218–231, 2004, ISSN: 01416359. DOI: 10.1016/j.precisioneng.2002.11.003.

[9] D. L. Blanding, "Exact Constraint Web Handling," Jan. 1999. DOI: 10.1115/1.800857_ch8. eprint: https://asmedigitalcollection.asme.org/book/chapter-pdf/2798927/800857_ch8.pdf. [Online]. Available: https://doi.org/10.1115/1.800857%5C_ch8.

[10] A. H. Slocum, "Kinematic couplings for precision fixturing-Part I: Formulation of design parameters," *Precision Engineering*, vol. 10, no. 2, pp. 85–91, 1988, ISSN: 01416359. DOI: 10.1016/0141-6359(88)90005-0.

[11] M. L. Culpepper, B. S. M. Engineering, A. H. Slocum, T. Supervisor, and A. a. Sonin, "Design and Application of Compliant Quasi-Kinematic Couplings," p. 198, 2000. [Online]. Available: http://pergatory.mit.edu/kinematiccouplings/documents/Theses/culpepper_thesis/quasi_kinematic_couplings.pdf.

[12] M. L. Culpepper, M. V. Kartik, and C. Dibiasio, "Design of integrated eccentric mechanisms and exact constraint fixtures for micron-level repeatability and accuracy," *Precision Engineering*, vol. 29, no. 1, pp. 65–80, 2005, ISSN: 01416359. DOI: 10.1016/j.precisioneng.2004.05.007.

[13] A. J. Hart, A. Slocum, and P. Willoughby, "Kinematic coupling interchangeability," *Precision Engineering*, vol. 28, no. 1, pp. 1–15, Jan. 2004, ISSN: 01416359. DOI: 10.1016/S0141-6359(03)00071-0.

[14] L. C. Hale, "Friction-Based Design of Kinematic Couplings," *Proceedings ASPE*, pp. 45–48, 1998.

[15] P. script Schmiechen, *Design of precision kinematic systems.pdf*, 1992.

[16] C. H. Schouten, P. C. Rosielle, and P. H. Schellekens, "Design of a kinematic coupling for precision applications," *Precision Engineering*, vol. 20, no. 1, pp. 46–52, Jan. 1997, ISSN: 01416359. DOI: 10.1016/s0141-6359(97)00002-0.

[17] F. Patti and J. M. Vogels, "Self-alignment of kinematic couplings: Effects of deformations," *Precision Engineering*, vol. 60, pp. 348–354, Nov. 2019, ISSN: 01416359. DOI: 10.1016/j.precisioneng.2019.08.013.

[18] A. H. Slocum, "Design of three-groove kinematic couplings," *Precision Engineering*, vol. 14, no. 2, pp. 67–76, 1992, ISSN: 01416359. DOI: 10.1016/0141-6359(92)90051-W.

[19] L. C. Hale and A. H. Slocum, "Optimal design techniques for kinematic couplings," *Precision Engineering*, vol. 25, no. 2, pp. 114–127, Apr. 2001, ISSN: 01416359. DOI: 10.1016/S0141-6359(00)00066-0.

[20] P. Schmiechen and A. Slocum, "Analysis of kinematic systems: A generalized approach," *Precision Engineering*, vol. 19, no. 1, pp. 11–18, 1996, ISSN: 01416359. DOI: 10.1016/0141-6359(96)00001-3.

[21] K. B. Shimoga, "Robot grasp synthesis algorithms: A survey," *International Journal of Robotics Research*, vol. 15, no. 3, pp. 230–266, 1996, ISSN: 02783649. DOI: 10.1177/027836499601500302.

[22] N. S. Pollard and T. Lozano-Perez, "Grasp stability and feasibility for an arm with an articulated hand," pp. 1581–1585, 1990. DOI: 10.1109/robot.1990.126234.

[23] A. T. Miller and P. K. Allen, "Examples of 3D grasp quality computations," *Proceedings - IEEE International Conference on Robotics and Automation*, vol. 2, no. May, pp. 1240–1246, 1999, ISSN: 10504729. DOI: 10.1109/robot.1999.772531.

[24] C. Borst, M. Fischer, and G. Hirzinger, "Fast and robust grasp planner for arbitrary 3D objects," *Proceedings - IEEE International Conference on Robotics and Automation*, vol. 3, no. May, pp. 1890–1896, 1999, ISSN: 10504729. DOI: 10.1109/robot.1999.770384.

[25] E. Chinellato, A. Morales, R. B. Fisher, and A. P. del Pobil, "Visual quality measures for characterizing planar robot grasps," *IEEE Transactions on Systems, Man and Cybernetics Part C: Applications and Reviews*, vol. 35, no. 1, pp. 30–41, 2005, ISSN: 10946977. DOI: 10.1109/TSMCC.2004.840061.

[26] K. Lakshminarayana, "MECHANICS OF FORM CLOSURE.," in *American Society of Mechanical Engineers (Paper)*, 1978.

[27] X. Markenscoff and C. H. Papadimitriou, "Optimum grip of a polygon," *International Journal of Robotics Research*, vol. 8, no. 2, pp. 17–29, 1989, ISSN: 02783649. DOI: 10.1177/027836498900800202.

[28] J. W. Jameson, "Analytic techniques for automated grasps," no. Dept. of Mechanical Engineering, 1985.

[29] R. J. Dawson, "On the mobility of bodies in Rn," *Mathematical Proceedings of the Cambridge Philosophical Society*, vol. 98, no. 3, pp. 403–412, 1985, ISSN: 14698064. DOI: 10 . 1017 / S0305004100063611.

[30] V.-D. Nguyen, "Constructing Force-Closure Grasps," Tech. Rep.

[31] B. S. Baker, S. Fortune, and E. Grosse, "Stable Prehension With Three Fingers.," *Conference Proceedings of the Annual ACM Symposium on Theory of Computing*, vol. 0, pp. 114–120, 1985, ISSN: 07349025. DOI: 10.1145/22145.22158.

[32] K. J. Waldron, "The constraint analysis of mechanisms," *Journal of Mechanisms*, vol. 1, no. 2, pp. 101–114, 1966, ISSN: 00222569. DOI: 10.1016/0022-2569(66)90016-4.

[33] C. Ferrari and J. Canny, *Planning Optimal Grasps*, 1999.

[34] J. W. Li, H. Liu, and H. G. Cai, "On computing three-finger force-closure grasps of 2-D and 3-D objects," *IEEE Transactions on Robotics and Automation*, vol. 19, no. 1, pp. 155–161, 2003, ISSN: 1042296X. DOI: 10.1109/TRA.2002.806774.

[35] D. Ding, H. Kong, and S. Wang, "Computing 3-D Optimal Form-Closure Grasps * Form-Closure Grasp," no. April, pp. 3573–3578, 2000.

[36] Y. Zheng and W. H. Qian, "Limiting and minimizing the contact forces in multifingered grasping," *Mechanism and Machine Theory*, vol. 41, no. 10, pp. 1243–1257, 2006, ISSN: 0094114X. DOI: 10 . 1016/j.mechmachtheory.2005.11.001.

[37] M. A. Roa and R. Suárez, "Computation of independent contact regions for grasping 3-D objects," *IEEE Transactions on Robotics*, vol. 25, no. 4, pp. 839–850, 2009, ISSN: 15523098. DOI: 10 . 1109 / TRO . 2009.2020351.

[38] Y. Zheng, "An efficient algorithm for a grasp quality measure," *IEEE Transactions on Robotics*, vol. 29, no. 2, pp. 579–585, 2013, ISSN: 15523098. DOI: 10.1109/TRO.2012.2222274.

[39] S. Liu and S. Carpin, "Partial convex hull algorithms for efficient grasp quality evaluation," *Robotics and Autonomous Systems*, vol. 86, pp. 57–69, 2016, ISSN: 09218890. DOI: 10 . 1016 / j . robot . 2016 . 09 . 004. [Online]. Available: http://dx.doi.org/10.1016/j.robot.2016.09.004.

[40] S. Qiu and M. R. Kermani, "A new approach for grasp quality calculation using continuous boundary formulation of grasp wrench space," *Mechanism and Machine Theory*, vol. 168, no. April 2021, p. 104 524, 2022, ISSN: 0094114X. DOI: 10.1016/j.mechmachtheory.2021.104524. [Online]. Available: https://doi.org/10.1016/j.mechmachtheory.2021.104524.

[41] R. Graham, "An efficient algorithm for determining the convex hull of a finite planar set," *Computer*, vol. 1, pp. 132–133, 1972.

[42] M. A. Peshkin and A. C. Sanderson, "Reachable Grasps on a Polygon: The Convex Rope Algorithm," *IEEE Journal on Robotics and Automation*, vol. 2, no. 1, pp. 53–58, 1986, ISSN: 08824967. DOI: 10.1109/JRA.1986.1087030.

[43] T. Huynh, C. Lassez, and J. L. Lassez, "Practical issues on the projection of polyhedral sets," *Annals of Mathematics and Artificial Intelligence*, vol. 6, no. 4, pp. 295–315, 1992, ISSN: 10122443. DOI: 10.1007/BF01535523.

[44] B. Chazelle, "An optimal convex hull algorithm in any fixed dimension," *Discrete Computational Geometry*, vol. 10, no. 1, pp. 377–409, 1993, ISSN: 01795376. DOI: 10.1007/BF02573985.

[45] J. Ponce, S. Sullivan, J. D. Boissonnat, and J. P. Merlet, "On characterizing and computing three- and four-finger force-closure graphs of polyhedral objects," *Proceedings - IEEE International Conference on Robotics and Automation*, vol. 2, pp. 821–827, 1993, ISSN: 10504729. DOI: 10.1109/robot.1993.291933.

[46] R. Fonseca, "The ultimate planar convex hull algorithm?," vol. 15, no. 1, pp. 1–7, 2010, ISSN: ¡null¿. [Online]. Available: https://absalon.itslearning.com/file / fs_folderfile . aspx ? FolderFileID = 1855810 % 5Cnpapers2://publication/uuid/644BABBC-EF4F-41DC-95A7-3695C8A5489A.

[47] C. B. Barber, D. P. Dobkin, and H. Huhdanpaa, "The Quickhull Algorithm for Convex Hulls," *ACM Transactions on Mathematical Software*, vol. 22, no. 4, pp. 469–483, 1996, ISSN: 00983500. DOI: 10.1145/235815.235821.

[48] Y. Zheng and W.-h. Qian, "Improving grasp quality evaluation," *Robotics and Autonomous Systems*, vol. 57, no. 6-7, pp. 665–673, 2009, ISSN: 0921-8890. DOI: 10.1016/j.robot.2008.12.002. [Online]. Available: http://dx.doi.org/10.1016/j.robot.2008.12.002.

[49] A. Bicchi and V. Kumar, "Robotic grasping and contact: A review," *Proceedings-IEEE International Conference on Robotics and Automation*, vol. 1, pp. 348–353, 2000, ISSN: 10504729. DOI: 10.1109/ROBOT.2000.844081.

[50] H. Kruger and A. F. V. D. Stappen, "Partial Closure Grasps : Metrics and Computation," *2011 IEEE International Conference on Robotics and Automation*,

pp. 5024–5030, 2011. DOI: 10.1109/ICRA.2011.5980171.

[51] A. Sahbani, S. El-Khoury, and P. Bidaud, "An overview of 3D object grasp synthesis algorithms," *Robotics and Autonomous Systems*, vol. 60, no. 3, pp. 326–336, 2012, ISSN: 09218890. DOI: 10.1016/j.robot.2011.07.016. [Online]. Available: http://dx.doi.org/10.1016/j.robot.2011.07.016.

[52] M. A. Roa and R. Suárez, "Grasp quality measures: review and performance," *Autonomous Robots*, vol. 38, no. 1, pp. 65–88, 2015, ISSN: 15737527. DOI: 10.1007/s10514-014-9402-3.

[53] Reuleaux, *kinematics of machinery*. 1876.

[54] P. Somov, "Uber gebiete von schraubengeschwindigkeiten eines starren korpers bie verschiedener zahl von stutzflachen," *Z. Mathematik Physik*, vol. 45, pp. 245–306, 1900.

[55] Z. Li and S. S. Sastry, "Task-Oriented Optimal Grasping by Multifingered Robot Hands," *IEEE Journal on Robotics and Automation*, vol. 4, no. 1, pp. 32–44, 1988, ISSN: 08824967. DOI: 10.1109/56.769.

[56] N. S. Pollard, "Synthesizing grasps from generalized prototypes," *Proceedings - IEEE International Conference on Robotics and Automation*, vol. 3, no. April, pp. 2124–2130, 1996, ISSN: 10504729. DOI: 10.1109/robot.1996.506184.

[57] C. Borst, M. Fischer, and G. Hirzinger, "Grasp planning: How to choose a suitable task wrench space," *Proceedings - IEEE International Conference on Robotics and Automation*, vol. 2004, no. 1, pp. 319–325, 2004, ISSN: 10504729. DOI: 10.1109/robot.2004.1307170.

[58] M. Strandberg, B. Wahlberg, and S. Member, "A Method for Grasp Evaluation Based on Disturbance Force Rejection," pp. 461–469, 2006.

[59] A. Bicchi, "On the closure properties of robotic grasping," *The International Journal of Robotics Research*, vol. 14, no. 4, pp. 319–334, 1995.

[60] G. Strang, *Introduction to Linear Algebra*, Fourth. Wellesley, MA: Wellesley-Cambridge Press, 2009, ISBN: 9780980232714 0980232716 9780980232721 0980232724 9788175968110 8175968117.

[61] P. D. F. Pack, "Linear Algebra and Its Applications," *Linear Algebra and Its Applications*, vol. 373, no. SUPPL. 2003, ISSN: 00243795. DOI: 10.2307/2978065.

[62] M. Teichmann, "Grasp metric invariant under rigid motions," *Proceedings - IEEE International Conference on Robotics and Automation*, vol. 3, no. April, pp. 2143–2148, 1996, ISSN: 10504729. DOI: 10.1109/robot.1996.506187.

[63] H. Jeong and J. Cheong, "Evaluation of 3D grasps with physical interpretations using object wrench space," *Robotica*, vol. 30, no. 3, pp. 405–417, 2012, ISSN: 02635747. DOI: 10.1017/S0263574711000713.

[64] R. Bro, E. Acar, and T. G. Kolda, "Resolving the sign ambiguity in the singular value decomposition," *Journal of Chemometrics*, vol. 22, no. 2, pp. 135–140, 2008, ISSN: 08869383. DOI: 10.1002/cem.1122.

[65] H. Soemers, *Design principles for precision mechanisms*, English. Netherlands: University of Twente, 2010, ISBN: 978-90-365-3103-0.

[66] H. Asada and A. B. By, "Kinematic Analysis of Workpart Fixturing for Flexible Assembly with Automatically Reconfigurable Fixtures," *IEEE Journal on Robotics and Automation*, vol. 1, no. 2, pp. 86–94, 1985, ISSN: 08824967. DOI: 10.1109/JRA.1985.1087007.

[67] J. J. Bausch and K. Youcef-Toumi, "Kinematic methods for automated fixture reconfiguration planning," pp. 1396–1401, 1990. DOI: 10.1109/robot.1990.126198.

[68] L. P. Rusli, "DESIGN AND ANALYSIS OF MECHANICAL ASSEMBLY VIA KINEMATIC SCREW THEORY," 2008.

Appendix A.

A.1. Performance results: Algebraic measures

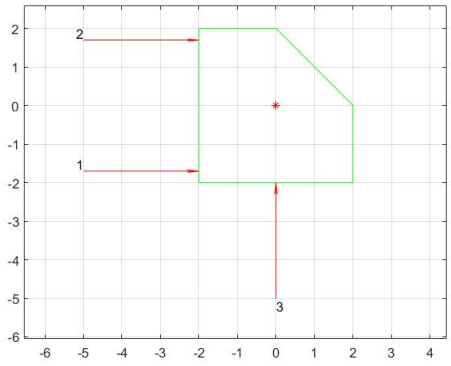

(a) σ_1 = 1.90, σ_2 = 1.27, σ_3 = 1.00

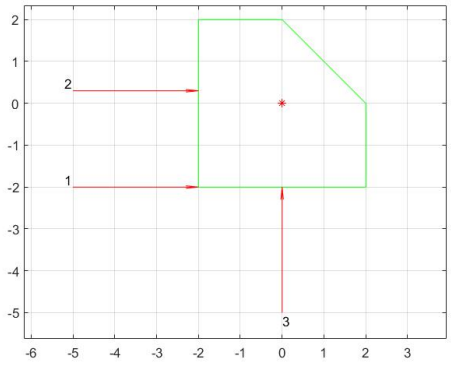

(b) σ_1 = 2.83, σ_2 = 1.41, σ_3 = 1.00

Figure A.1.1: Q_{msv}*: sub-optimal contact displacement, equal scoring*

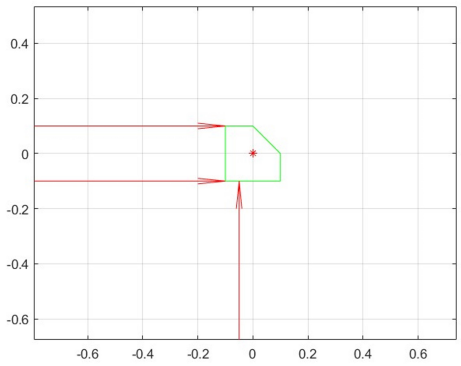

(a) $\sigma_1 = \sqrt{(2)}$, σ_2 = 1.00, σ_3 = 0.14

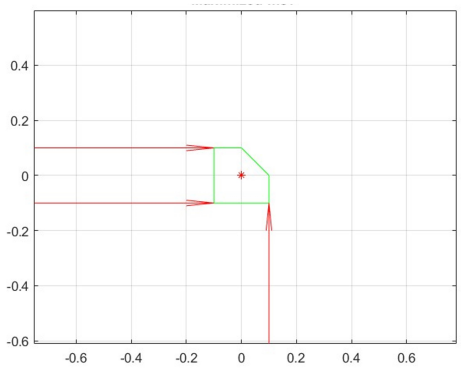

(b) $\sigma_1 = \sqrt{(2)}$, σ_2 = 1.00, σ_3 = 0.14

Figure A.1.2: Q_{msv}*: effect of scaling*

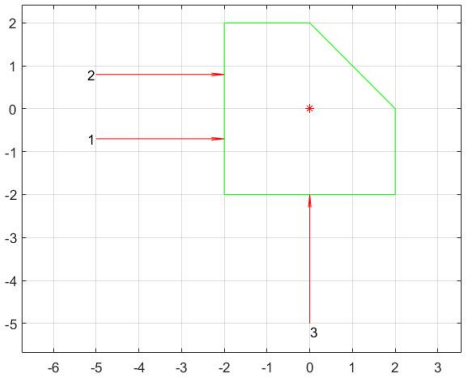

(a) $\sigma_1 = \sqrt{(2)}$, σ_2 = 1.00, σ_3 = 1.00

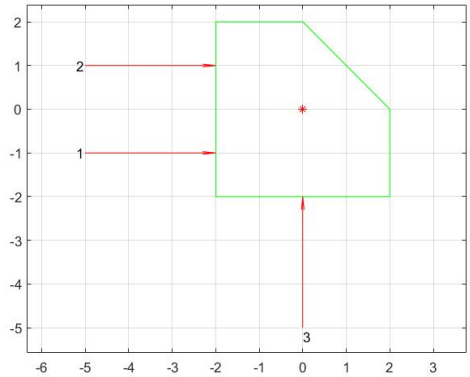

(b) $\sigma_1 = \sqrt{(2)}$, σ_2 = 1.00, $\sigma_3 = \sqrt{(2)}$

Figure A.1.3: Q_{gii}*: different moment arm, equal scoring*

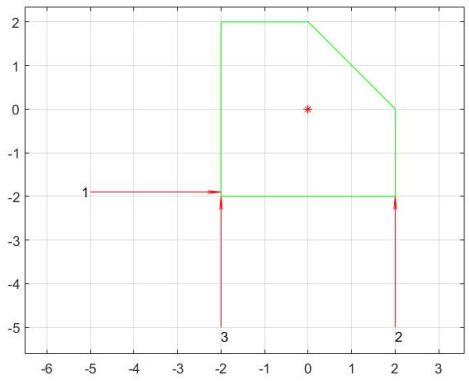

(a) σ_1 = 0.80, σ_2 = $\sqrt{(2)}$, σ_3 = 3.51

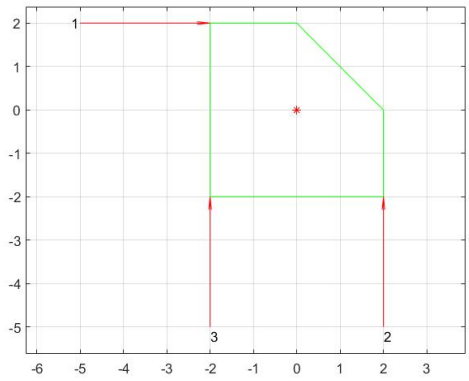

(b) σ_1 = 0.80, σ_2 = $\sqrt{(2)}$, σ_3 = 3.51

Figure A.1.4: Q_{vew}: *displaced force vector, equal scoring*

A.2. Performance results: Geometric measures

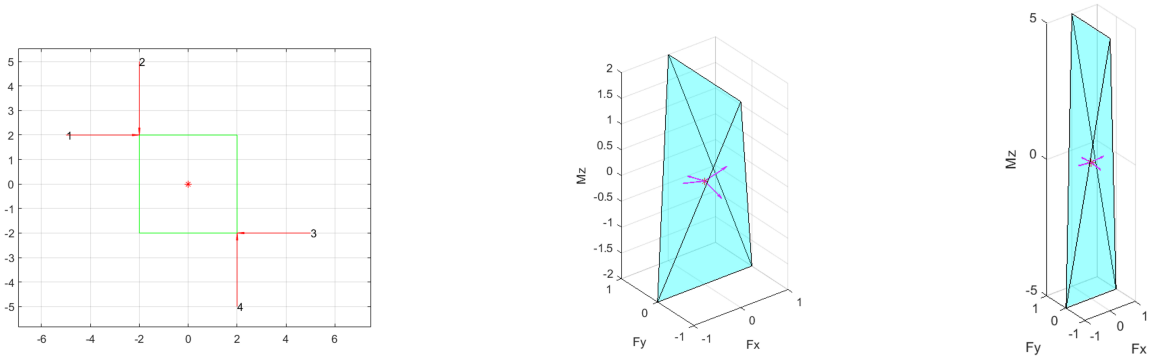

(a) Grasp **(b)** Hull of grasp (a) **(c)** equally rated grasp

Figure A.2.1: Q_{lrw} *:the effect of moment arm increase on hull*

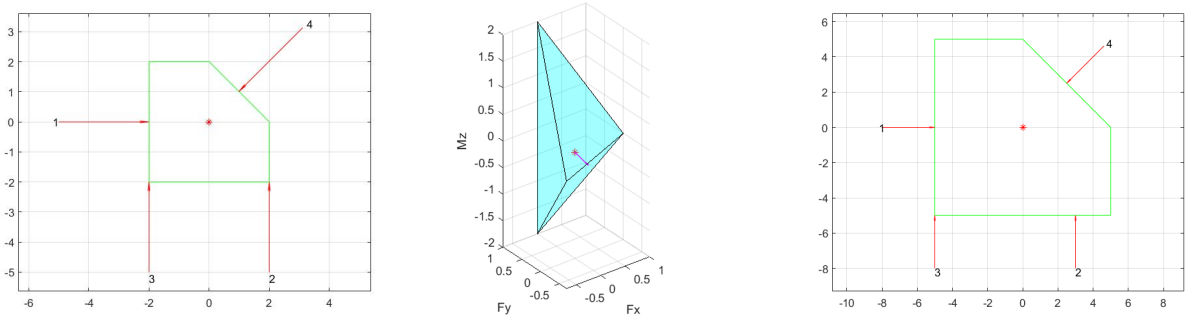

(a) Grasp **(b)** Radius: 0.4851 **(c)** sub-optimal contact placement

Figure A.2.2: Q_{lrw}*: the effect of focusing on weakest direction only*

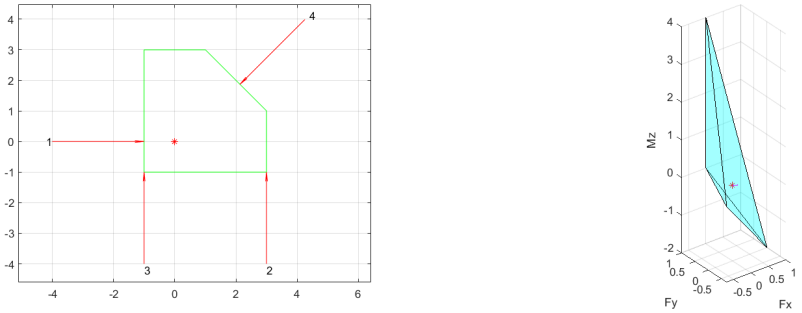

(a) Grasp **(b)** Radius: 0.165

Figure A.2.3: Q_{lrw}*: the effect of origin displacement*

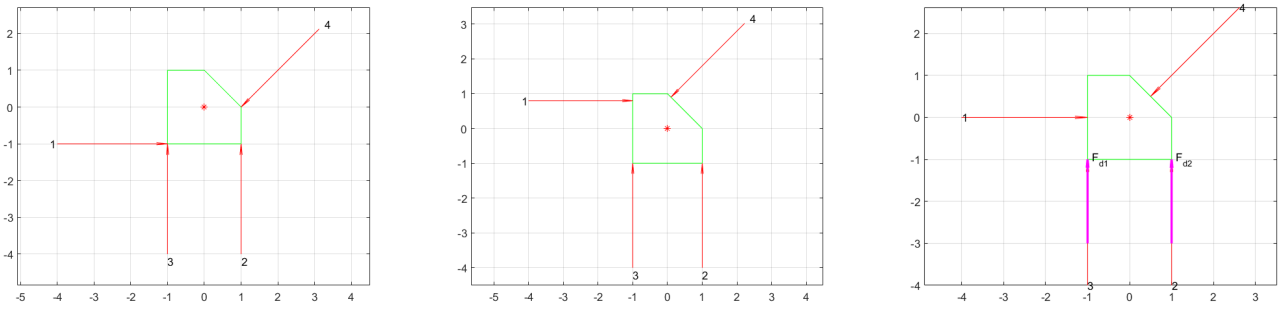

(a) Optimal result 1 **(b)** Optimal result 2 **(c)** Disturbance forces present

Figure A.2.4: *Q_{og}: range of equally rated configurations.*

Appendix B.
Case study results

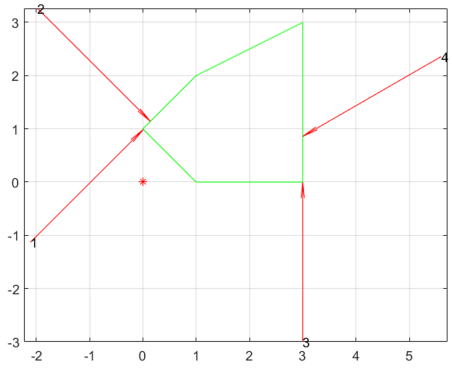

(a) Q_{og} result

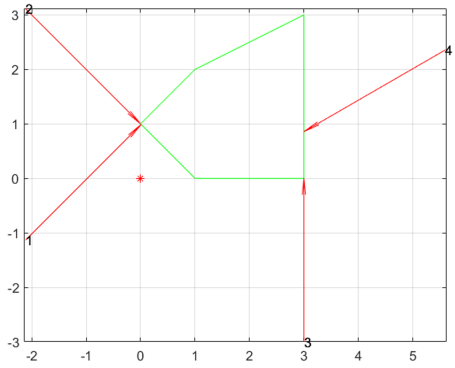

(b) Q_{lsm} result

Figure B.0.1: *v1*

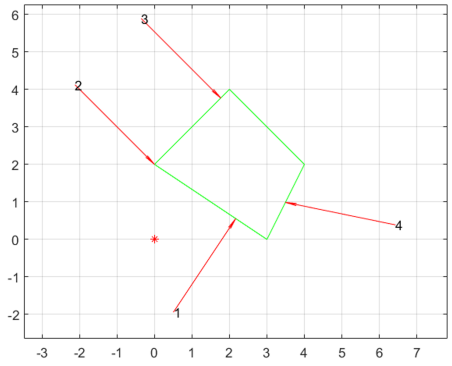

(a) Q_{og} result

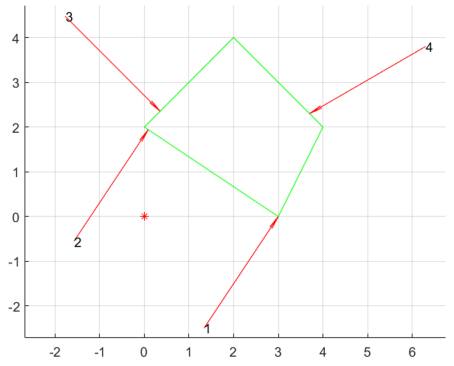

(b) Q_{lsm} result

Figure B.0.2: *v2*

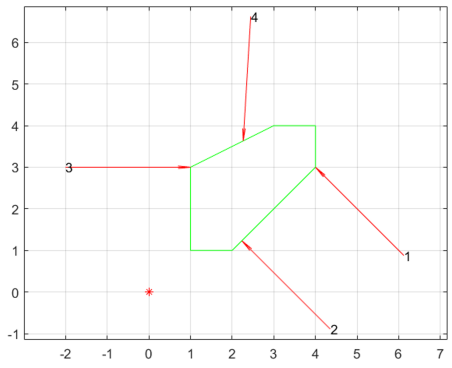

(a) Q_{og} result

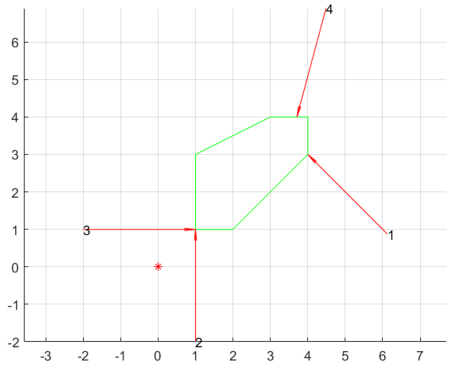

(b) Q_{lsm} result

Figure B.0.3: *v3*

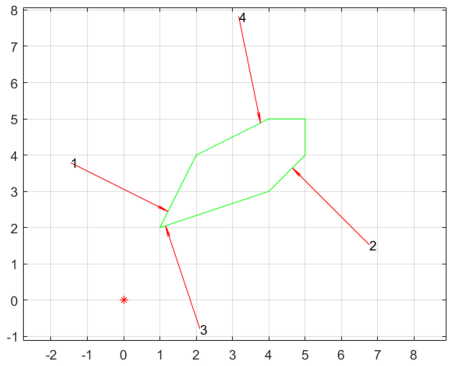

(a) Q_{og} result

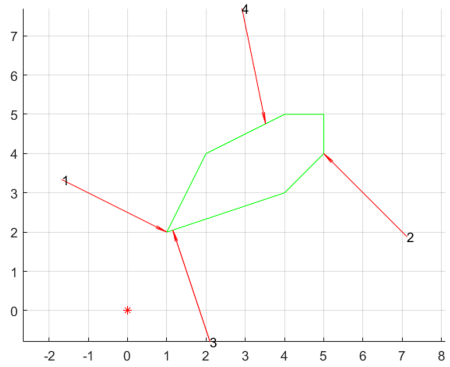

(b) Q_{lsm} result

Figure B.0.4: *v4*

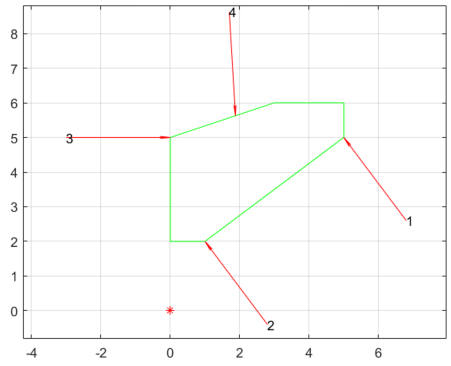

(a) Q_{og} result

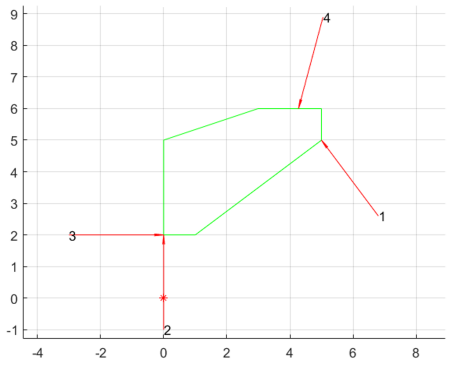

(b) Q_{lsm} result

Figure B.0.5: *v5*

B.1. Computation time analysis

Complexity of measures has been tested to get a general idea of computation ti

In this section the complexity of the measures is shown and tested, given that computation time can pose a serious bottleneck for the application of convex hull measures in particular, some insight is given using table 2. Theoretical complexity here is stated when known, versus an experimental section where the average time of 10.000 calculations implemented on the same set of configurations has been calculated. The computation time of the combined measure is dependent on the size of the nesting for set versus the size of contact set. An important side-note is that coding has only been marginally optimized for these computations. More advanced algorithms are available to calculate the computationally complex hull measures.

Measure	Complexity	
	Theoretical	Experimental
MSV	Omin([m,n])	7.8e-6
GII	Omin([m,n])	7.8e-6
VEW	Omin([m,n])	7.8e-6
RREF	O(mn(min[m,n]))	8.6e-5
LRW	O(nlog(n) - n^2)	3.9e-4
OGws	*	2.8e-4 - graph

TABLE 2: *computation time*

For measure Q_{og} the theoretical computation time is not given in literature. As shown in the experimental section, the computation time is largely dependent on the resolution of the calculations, as well as the way this measure is implemented. The OWS is generally comprised of a significantly larger set of wrenches, therefore calculating this convex hull dominates computation time. The effect of increasing the data set can be seen in figure B.1.1a, where a quadratic increase in computation time can be observed. Generally however, the same object and thus the same OWS will be subjected to different configurations to filter out the best one. In this case, the OWS can be calculated once and passed on in the search for the best GWS to enclose the OWS. This significantly reduces computation time, seen in figure B.1.1b.

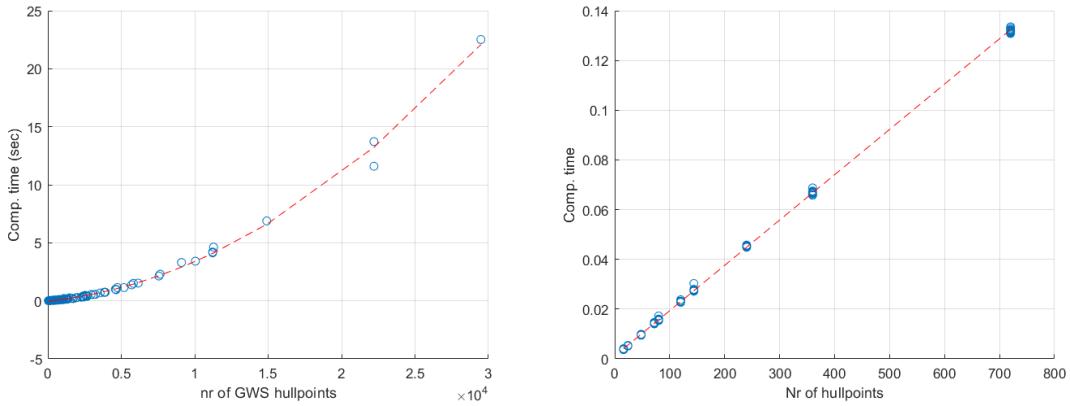

(a) OWS calculated **(b)** OWS given

Figure B.1.1: *Impact of calculating the convex hull of the object wrench space (OWS)*

B.2. Example calculations

B.2.1. RREF/nullspace + Q_{lsm}.

$$f_i = \frac{1}{\sqrt{n}} \tag{B.2.1}$$

$$Err = \frac{1}{n}\sum_{i=1}^{n}(f_i - x_i)^2 \tag{B.2.2}$$

The G matrix of configuration 16 and 17.

$$G = \begin{bmatrix} 1 & 1 & 0 & -0.866 \\ 0 & 1 & 1 & -0.500 \\ 2 & 1.6 & 2 & -2.559 \end{bmatrix} \tag{B.2.3}$$

Converting it to reduced row echelon form gives:

$$G = \begin{bmatrix} 1 & 0 & 0 & -0.433 \\ 0 & 1 & 0 & -0.433 \\ 0 & 0 & 1 & -0.500 \end{bmatrix} \tag{B.2.4}$$

Number of contacts (n) = 3
f_i = 0.577

Either the last row of the reduced form can be used for x_i, or the first 3 entries of the nullspace of the G matrix.

Nullspace approach gives:

$$x = null(G); \tag{B.2.5}$$

$$x = \begin{bmatrix} 0.340 \\ 0.340 \\ 0.392 \\ 0.784 \end{bmatrix} \tag{B.2.6}$$

scaled to unity gives equal entries as reduced form:
x_1 = 0.433, x_1 = 0.433, x_1 = 0.500

$$Err = \frac{1}{3}\sum_{i=1}^{3}(0.5 - x_i)^2 \tag{B.2.7}$$

Error = 0.01588

B.3. Experimental theory

The standard configuration seen in figure B.3.1 (L) is the grip which is being tested in this setup. The forces have been shifted along their line of action, which can be seen in the right picture of the figure.

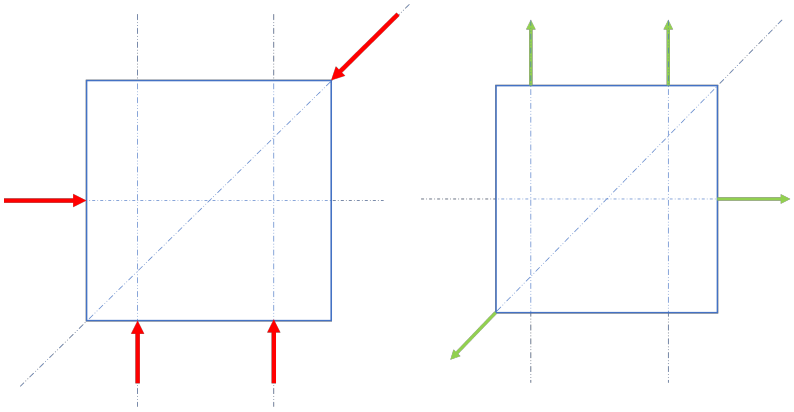

Figure B.3.1: *Compressive forces (L) Retractive forces (R)*

This way, a setup could be designed that made use of tensile force cables resembling the contact points. The benefit of this tensile setup is that it does not suffer from problems regarding friction and slip. As a trade off, the cables do need to be positioned and angled in an accurate manner. Figure B.4.4 shows a schematic of the build setup.

The position and direction vectors per contact resulted in the particular wrench matrix G, seen in (B.3.1).

$$G = \begin{bmatrix} 1 & 0 & 0 & -\sqrt{(2)}/2 \\ 0 & 1 & 1 & -\sqrt{(2)}/2 \\ -3 & 0 & 6 & 0 \end{bmatrix} \tag{B.3.1}$$

An example of the Q_{og} MATLAB model can be seen in figure B.3.2, where the weakest wrench is indicated as 'Wmin'. This disturbance force was also applied in a tensile manner.

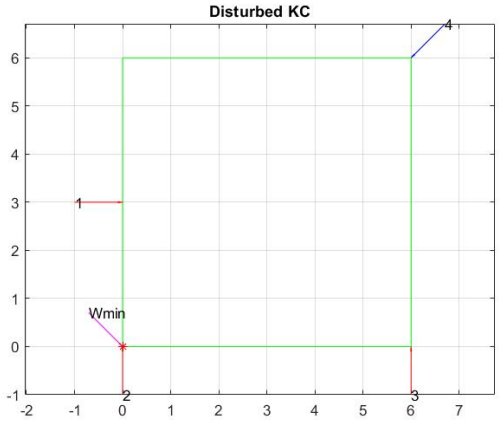

Figure B.3.2: *Disturbed coupling*

Given that the Q_{og} measure is a ratio without dimension, the magnitude of both input and measured forces can be arbitrarily selected. This is useful not only for increasing the amount of measures, but also to limit the impact of friction and cable stiffness on the measurements, which are effects that occur in the low and higher regions of loading forces resp. The correctness of the ratio can be tested by preloading the system with a chosen magnitude of contact forces, by simply scaling the magnitude of the contact vectors that make up matrix G. Equation B.3.2 provides the 'weights' or actual force per contact that is required to hold a particular setup in equilibrium.

$$null(G) = x \text{ with } |x| = 1; \tag{B.3.2}$$

The null-space of G provides a linear dimension of solutions, meaning it can be scaled in order to resemble the correct equilibrium forces that match the chosen magnitude.

Figure B.3.3 shows a simplified example of how the Q_{og} measure works, where the red dot indicates the intersection between the hull(GWS) of the grasp in blue and the disturbance force 'Fd', which is part of a large set of disturbance forces that make up the OWS. This intersection then provides the ratio of which the disturbance force needs to be scaled in order to fit within the hull of the grip. If disturbance forces remain within the hull of the grip, equilibrium is maintained.

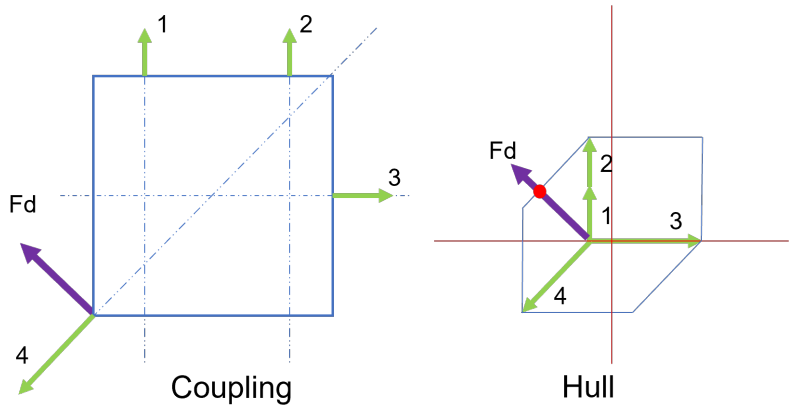

Figure B.3.3: *Coupling and Hull*

Even though the smallest of factors is used as measure, all scale factors belonging to the disturbance forces can be used for testing the correctness of the model. This way, plenty of measures can be conducted from only 1 grip.

When equilibrium is lost, it means that a contact loses it's grip and does not contribute to the equilibrium anymore. In a tensile setup this translates to a zero force magnitude, which can be visualised by readings of tensile force sensors in between the suspending cables.

B.4. Experiment implementation

The Load cells were powered by 4 CPJ analog transmitters. A Texas Instruments NI-USB6008 was used to read the values from the load cells, after which Labview software was used to graph and display the results.

The top 2 force sensors were first given an offset in order to compensate for the weight of the suspended block, which includes set screws with aluminum wire fixation rings in order to connect the wires with the block. A level and a triangle ruler combined with the plumb line were used to level out the block in the undisturbed situation as accurate as possible before moving on to the measurements.

The brass connectors allow the nylon lines to be tightened towards the frame whilst leaving the load cells untwisted due to the freedom of rotation of the M3 bolts. This way, equilibrium of forces was established. The values for force equilibrium were calculated by equation B.3.2. Given that the null solution has 1 dimension, the values can be scaled linearly for measurements with higher forces/pretension.

When leveled out, the analog force gauge was brought into position. The angle of the disturbance force given by the Q_{og} was calculated, and the pulley system guiding the disturbance force wire was shifted across the frame until the desired angle was achieved. By carefully shifting the analog meter across the aluminum profile, the cord was brought under tension. Life readings of the force sensors using Labview provided insight regarding the stability of the system. A zero force reading in one of the contacts indicates the tipping point of the grip becoming unstable.
The setup and some important features can be seen in figures B.4.4-B.4.3.

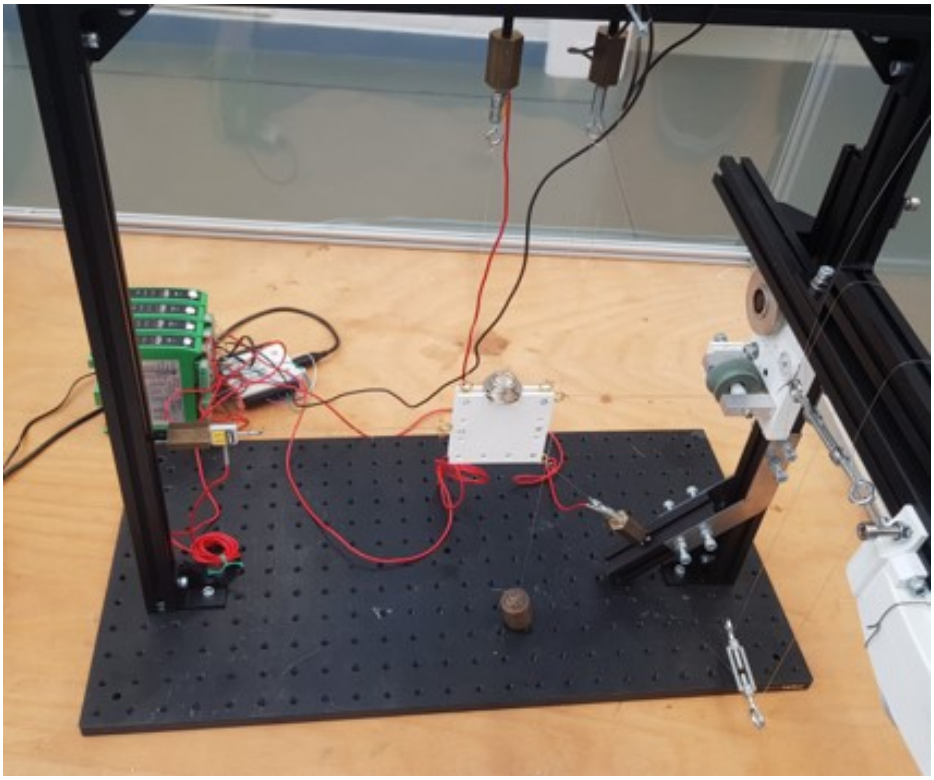

Figure B.4.1: *Set up*

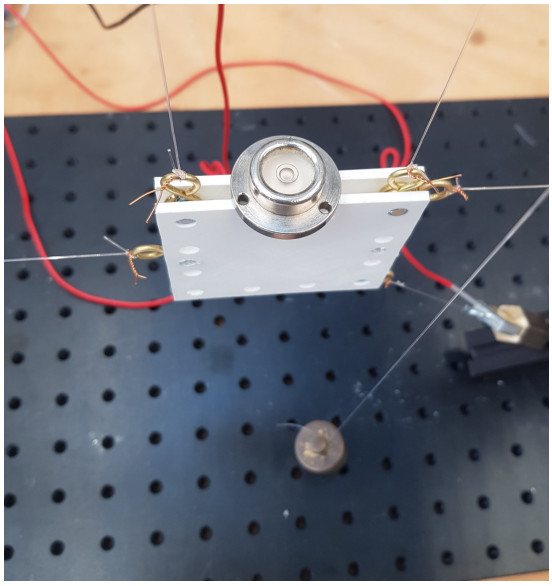

(a) Horizontal

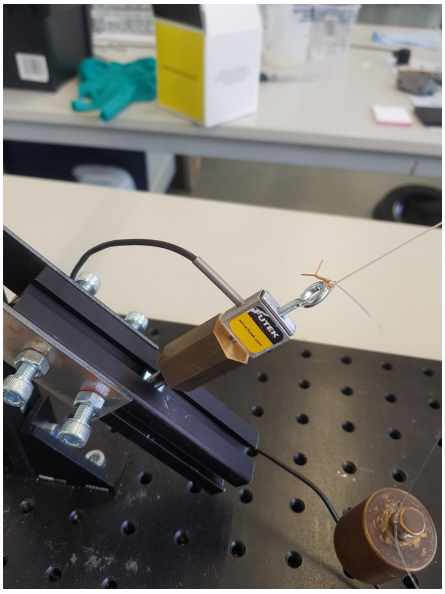

(b) Load cell

Figure B.4.2: *setup details*

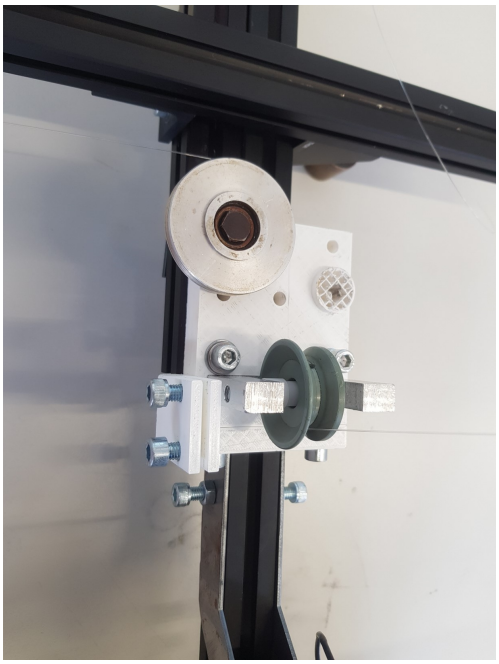

(a) pulley

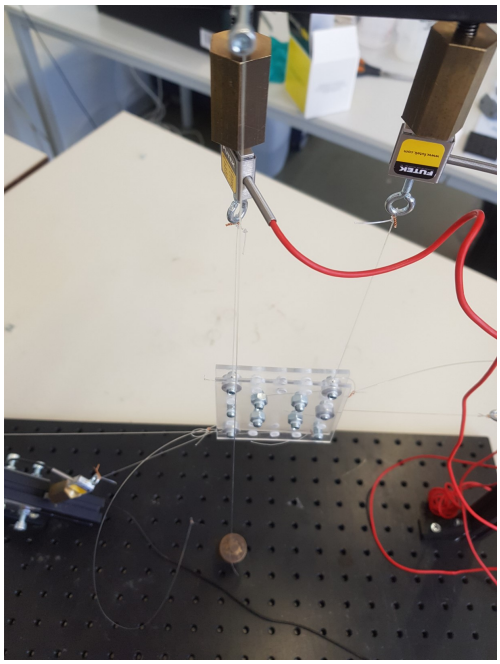

(b) plumb line

Figure B.4.3: *setup details*

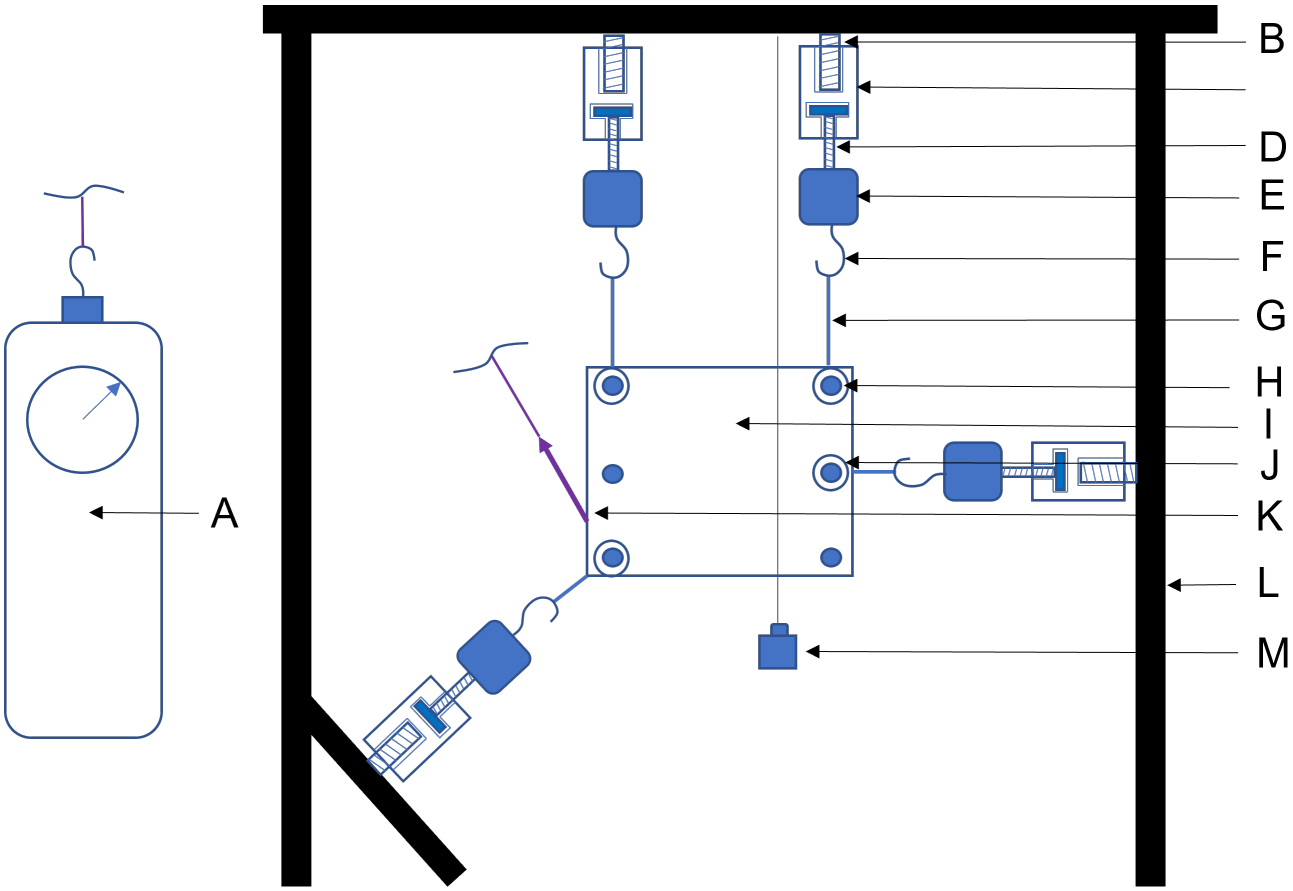

Figure B.4.4: *experimental setup*

1) A SN10 Analog force sensor
2) B Set screw
3) C Brass connector
4) D M3 screw
5) E Futek 40N Load cell
6) F M3 screwhook
7) G Nylon wire 0.5mm
8) H Set screw
9) I Lasercut plexiglass
10) J Aluminum wire fixation ring
11) K Disturbance force wire (Nylon)
12) L Aluminum profile frame
13) M Plumb line